Fall 12-2020

Nanosecond Stimulation and Defibrillation of Langendorff-Perfused Rabbit Hearts

Johanna Neuber
Old Dominion University, juneuber3@gmail.com

NANOSECOND STIMULATION AND DEFIBRILLATION OF LANGENDORFF-PERFUSED RABBIT HEARTS

by

Johanna Neuber
M.S. May 2016, Old Dominion University
B.S. May 2014, University of Texas at Austin

A Dissertation Submitted to the Faculty of
Old Dominion University in Partial Fulfillment of the
Requirements for the Degree of

DOCTOR OF PHILOSOPHY

BIOMEDICAL ENGINEERING

OLD DOMINION UNIVERSITY
December 2020

Approved by:

Shu Xiao (Director)

Christian Zemlin (Member)

Andrei Pakhomov (Member)

Tom Vernier (Member)

ABSTRACT

NANOSECOND STIMULATION AND DEFIBRILLATION OF LANGENDORFF-PERFUSED RABBIT HEARTS

Johanna Neuber
Old Dominion University, 2020
Director: Dr. Shu Xiao

The search for novel defibrillation methodologies focuses on minimizing deposition of energy to the heart, as this is an indicator for side effects including pain and tissue death. In this work, we investigate the effect of reducing the duration of the applied shocks from low milliseconds to the nanosecond range.

300 ns defibrillation was observed and confirmed to require lower energy than monophasic shocks by almost an order of magnitude with no tissue damage. Additionally, the safety factor, the ratio of median effective doses for electroporative damage and defibrillation, was similar for both durations. To predict how defibrillation shocks of any duration affect the heart, the stimulation strength-duration curve from 200 ns to 10 ms was determined.

To investigate whether high frequency trains of nanosecond shocks (MHz compression) are capable of reducing the electric field and energy of defibrillation, they were compared with a single shock of the same duration. The average voltage for the pulse trains was slightly lower than for long shocks, but the energy almost doubled.

Finally, to understand how shocks even shorter than 300 ns perform, we attempted to determine the defibrillation threshold of 60 ns shocks. Both the estimated electric field and energy were markedly higher than for 300 ns. We also investigated the stimulation threshold of 60 ns shocks

followed by a negative phase of varying amplitude and showed that the negative phase reduces the ability of the shocks to stimulate.

In conclusion, this work contributes to the understanding of how nanosecond shocks interact with cardiac tissues. It shows that 300 ns defibrillation is effective and similarly safe as 10 ms shocks, while requiring almost an order of magnitude less energy. The stimulation strength-duration curve for cardiac tissue follows the same trend, with lower than expected thresholds for nanosecond shocks. However, low voltage MHz compressed nanosecond shocks are similarly effective as long shocks of the same duration, indicating that the greater efficacy of nanosecond defibrillation is linked to the effects of high voltage. Finally, investigations in 60 ns shocks show defibrillation and stimulation are possible, and that bipolar cancellation occurs in cardiac tissue.

I dedicate this thesis:

To my angels, Daniel and David: who are watching over me

To my family: who supported and encouraged me

To my partner, Thomas: who helps me believe in myself

To my second family, the Careys: who welcomed me and gave me strength

ACKNOWLEDGEMENTS

I would like to acknowledge the people who have helped me on this journey, though there have been many hurdles to overcome.

Firstly, I would like to thank my partner, Thomas, though he hates that word. We are partners in life, and I have lost track of the times he has lifted me up and helped me remember that I am capable of anything, so long as I set my mind to it.

I would also like to express my appreciation for my mentor, Christian Zemlin. It has been a challenging 5 years, but never once has he been anything but supportive and understanding. I experienced many personal losses, which affected my productivity and mental wellbeing, but he took everything in stride and never gave up on me. I count myself blessed to have such an encouraging and wise advisor who saw me through to the very end, even from a distance.

I also credit my best friend Hollie for helping me find my path forward even when I couldn't see my own way. She provided encouragement and support, and shared her journey through the struggles of graduate life. I am eternally grateful to have found someone likeminded, who understands the value of life outside of school and the workplace.

I would also like to thank Dr. Xiao and Carol for providing the technical support for many of my experiments, and particularly to Dr. Xiao for being available for questions after my advisor moved away. Dr. Pakhomov and Dr. Vernier have also been instrumental in providing feedback and their expertise in their fields, for which I will be forever grateful.

Without these persons, and countless others among my family and friends, I would not be where I am today. It truly does take a village.

NOMENCLATURE

APD	Action Potential Duration
AV	Atrioventricular
C	Velocity of Light in Vacuum
DI	Diastolic Interval
ECG	Electrocardiogram
R_{charge}	Charging Resistor
ε	Permittivity
VF	Ventricular Fibrillation
SA	Sino Atrial
nsPEF	Nanosecond Pulsed Electric Field
V_{BD}	Breakdown Voltage
ε_R	Relative Permittivity
TTC	Triphenyl Tetrazolium Chloride
PI	Propidium Iodide
Ω	Ohms

TABLE OF CONTENTS

Page

LIST OF FIGURES

Figure Page

CHAPTER 1:

INTRODUCTION

Short, intense electric shocks have long been the method of choice to terminate ventricular fibrillation [1-5]. The current clinical standard is to deliver truncated exponential biphasic pulses of approximately 10 ms duration [6-9], either via electrode panels placed on the thorax [10] or, in patients known to be at risk for fibrillation, via an implanted defibrillation device with electrodes close to and inside the heart [11].

Since the time when defibrillation was introduced, particular effort has been put into finding shock wave forms that would allow effective defibrillation at lower energies [12, 13], thereby reducing side effects such as increased morbidity and mortality, anxiety, pain, and cell damage [14-16]. This research led to the replacement of the original monophasic, truncated exponential waveforms by the biphasic waveforms that are used today [17-19]. Triphasic [20] and quadriphasic [21] as well as biphasic shocks with an ascending first phase [22] have also been investigated for low energy properties.

1.1 Electrical Activity of the Heart

Cardiac activity is controlled by electrical signals that are generated on a cellular level, spread over the heart, and initiate cardiac contraction. The electric signals originate from a potential difference across the cell membrane which are caused by differing ion concentrations in the extracellular medium and the cytoplasm. As ion channels embedded in the membrane open and

close, the resulting transmembrane current changes the potential difference across the membrane, leading to propagation of electrical signals. In a membrane at the resting state, if the ion concentrations are known, the resting membrane potential can be found using the equation for the Nernst potential:

$$V_{membrane} = \frac{RT}{zF} ln \frac{[ion\ outside\ the\ cell]}{[ion\ inside\ the\ cell]} \qquad \text{Equation 1}$$

Where R is the universal gas constant, T is the temperature in Kelvin, z is the charge of the ion, and F is the Faraday constant.

This equilibrium membrane potential is about -90 mV for cardiomyocytes and is maintained primarily by the sodium-potassium pump as well as the sodium-calcium exchanger that results in a sodium and calcium concentration outside the cell that is higher than the concentration inside the cell and a potassium concentration that is larger inside the cell. When cells are excited, a change in the transmembrane voltage that exceeds the stimulation threshold sets off a cascade reaction. Sodium channels open, allowing sodium to flood into the cell, effectively depolarizing the membrane. See Figure 1. Sodium channels then close, and the opening of potassium channels then allows potassium to leave the cell resulting in a notch after the peak. Calcium channels then open, and calcium influx balances out potassium efflux, resulting in a plateau in the transmembrane voltage. Finally, potassium leaves the cell while the calcium channels close, repolarizing the membrane.

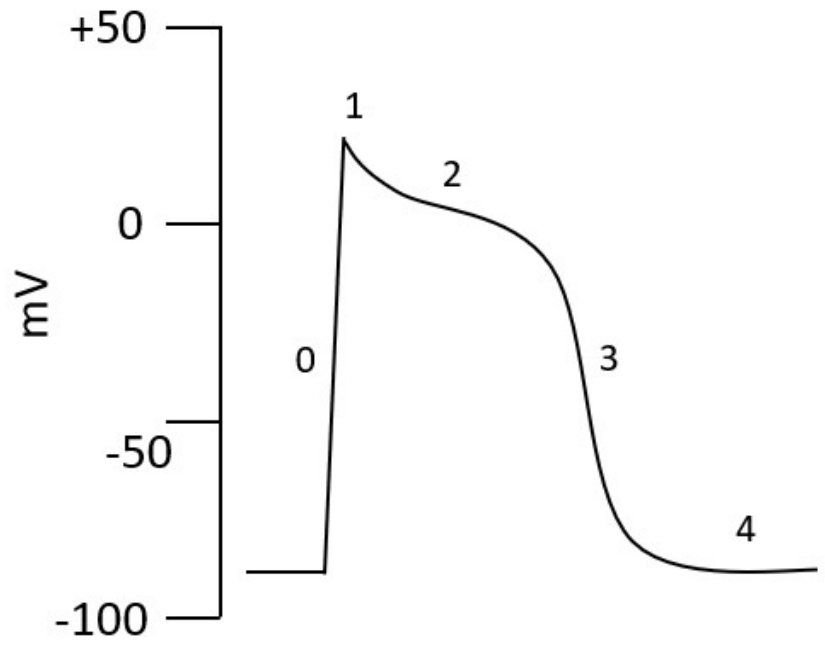

Figure 1. A representative graph of a cardiac action potential. After the membrane is stimulated to a voltage above the activation threshold, sodium channels open, and sodium enters the cell (Phase 0). Sodium channels then close while potassium channels open and potassium leaves the cells (Phase 1). In Phase 2, calcium influx balances the potassium efflux, resulting in a plateau of the action potential. During Phase 3, Calcium channels then close and potassium efflux drives the potential back to its resting potential (Phase 4).

In cardiac tissue, excitation and contraction are closely linked. During an action potential, calcium enters the cell. Ca^{+2} then binds to receptors on the sarcoplasmic reticulum, which then open and release even more calcium into the cytoplasm. This Ca^{+2} then activates myofilaments, causing contraction of the muscle cell.

For a basic electrophysiological understanding, the lipid bilayer that composes the cell membrane of the cells of all living organisms can be considered as a leaky capacitor. The membrane provides the capacitance and the ion channels provide a leak current path (see Figure

2). The voltage created by the ion gradient across the membrane is known as the resting membrane potential. If you apply a voltage to a passive membrane with all channels closed, you would see charging of the membrane analogous to a resistor-capacitor circuit. After the transmembrane voltage reaches a certain threshold, a cascade of opening and closing channels results that ultimately produces an action potential. This excitation cascade has been thoroughly studied and modeled [23, 24]. However, once charging voltages on the order of 1 V are reached, the story is complicated by the formation of pores in the cell membrane, introducing another path for current (ions) to flow.

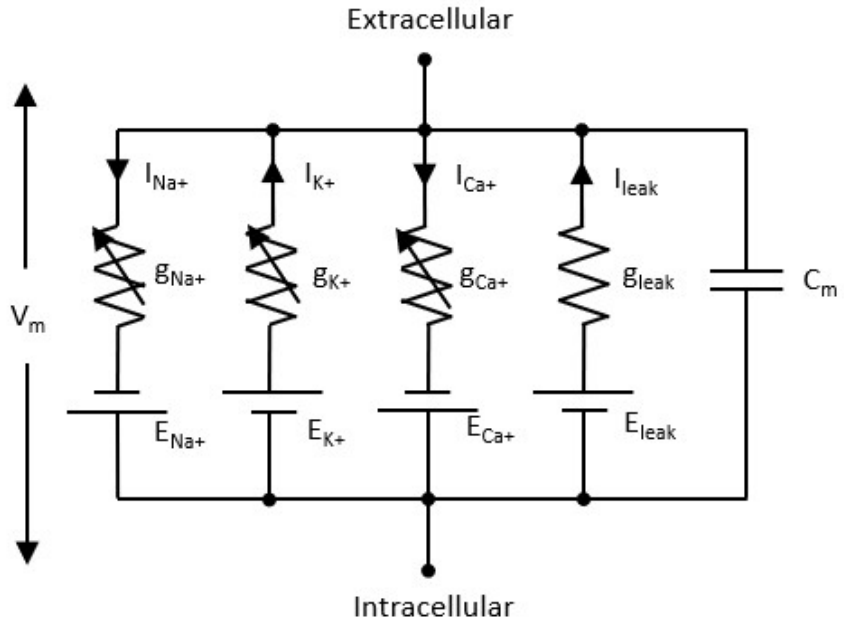

Figure 2. Model of a patch of cell membrane using resistors and capacitors. A parallel circuit is represented for each ion, as well as any leakage, where g is the conductivity of the membrane for each

ion, with it being variable in the case of sodium and potassium due to specific ion channels, E is the contribution of the concentration gradient of each ion to the transmembrane potential, and I is the current caused by movement of each ion, with the arrow pointing down the concentration gradient.

Since the electrical behavior of capacitors and resistors is well established, this cell membrane model allows us to predict the effects of an externally applied electric field. Each membrane patch will have an associated time constant (τ), which is the product of the resistance and capacitance, and will exhibit the exponential charging behavior of an R-C circuit. Determining where this model breaks down will also allow for insight into alternate charging mechanisms or electroporation effects.

1.2 Defibrillation technology

When the heart is functioning normally, the sinoatrial node spontaneously depolarizes. The excitation signal is then propagated through the atria which contract synchronously, pumping blood to fill the ventricles. The atria and the ventricles are electrically connected via the atrioventricular (AV) node, which slows conduction of excitation. After a short delay while the ventricles fill with blood, the excitation signal is passed through the AV node, and passes along the Purkinje fibers, allowing for synchronous contraction of the ventricles, which pumps blood from the left atrium through the aorta to the body and from the right atrium to the lungs where the blood is oxygenated.

Arrhythmias occur when there is a malfunction of some aspect of the conduction-excitation system. These can be problematic, such as atrial fibrillation (AF) or ventricular tachycardia (VT), or fatal, such as ventricular fibrillation (VF).

The most serious arrhythmias are caused by re-entrant waves of excitation. Many nonconducting structures are connected to the heart, such as valves, pulmonary arteries and veins, and the vena cava and aorta. In some cases, a wave of excitation can anchor to one of these structures, and begin revolving around it. Instead of being excited once the SA or AV nodes depolarize, the tissue is reactivated once the excitation front rotates a full 360° at returns to the same region. In the atria, this results in asynchronous contraction, which is then propagated through the AV node, causing irregular or fast synchronous contraction of the ventricles, which do not allow the atria and ventricles to work at their maximum capacity, since there is not enough time for the ventricles to fill properly with blood.

During ventricular fibrillation, there is no synchronous electrical activity. Instead, cardiomyocytes exhibit disorganized excitation, and the heart tissue quivers, unable to pump blood to the body. This is a potentially fatal arrhythmia and must be quickly treated to save a patient's life.

In atria, ablation procedures to connect the nonconducting structures with ablated, nonconducting lesions are often recommended, as well as medication to reduce the incidence of fibrillation and cardioversion. While ablation kills some of the atrial tissue, this killing is justified if the atrial fibrillation can be eliminated, and patients are able to live healthy lives after the procedure.

For ventricular tachycardia and fibrillation, defibrillation is the method of choice for terminating the arrhythmia. The aim of defibrillation is to apply enough electrical energy to the heart to uniformly excite most of the organ. After the tissue is excited, there is a refractory period, and this process ideally will have stopped any re-entrant waves and synched the action potentials so

that the SA node can take over and return the heart to sinus rhythm. For an acute case, external paddles are placed on the thorax and an electrical shock is applied. In the case where a patient is at risk of repeated VF episodes, an implantable defibrillator can be used to detect instances of fibrillation and apply defibrillation shocks to restore normal heart rhythm.

1.3 Nanosecond pulsed electric fields

Advances in pulsed power engineering over the last few decades as well as research into the bioeffects of nanosecond pulsed electric fields have opened up the possibility of nanosecond defibrillation, a potentially superior alternative to conventional, millisecond defibrillation. Nanosecond shocks, similarly to millisecond shocks, can excite nerve and muscle cells, as well as cardiomyocytes [25-27]. There is some evidence that stimulation with such short shocks does not rely on movement of ions to reach the threshold transmembrane voltage [28, 29], allowing for potentially more uniform excitation and electric field distribution throughout the myocardium. This would also minimize the effect of tissue inhomogeneities and reduce the risk of reversion to ventricular fibrillation [30, 31].

Electroporation is the cause of many of the adverse side effects of millisecond defibrillation [2, 16]. Formation of pores in the cell membrane will cause cells to depolarize and prevent the cell from maintaining the ion balance essential to proper functionality and excitation. This can result in the reduction of action potential amplitude, swelling, and cell death. However, electroporation, depending on the severity, may also be anti-arrhythmic and assist defibrillation [2, 16]. Promisingly, the effective diameter of pores induced by nanosecond shocks is smaller than for millisecond shocks, and is limited to 1-1.5 nm [31-34], which will minimize leakage from the

membrane while preserving reduced excitability. Since shocks are of a very short duration, transport of solutes by electrophoretic components is virtually eliminated [35]. Nanosecond shocks can also inhibit sodium and calcium voltage-gated channels [36, 37], which would assist the anti-arrhythmic properties of the shocks.

All of these factors combine to make nanosecond pulsed electric fields a very promising defibrillation modality which will be thoroughly explored in this dissertation.

1.4 Overview

This dissertation focuses on a new approach to defibrillation, which is to use shocks that are much shorter than conventional pulses, i.e. nanosecond duration pulses.

In Chapter 3, we demonstrate that 300 ns defibrillation is possible at lower energies than 10 ms defibrillation. In these experiments, no electroporative damage as indicated by propidium iodide fluorescence was observed for a single defibrillation-strength shock. Additionally, there was no baseline shift in optical mapping traces or changes in action potential duration, only a brief increase in diastolic interval for one beat after the defibrillation shock was applied.

In Chapter 4, electric field modeling in combination with a histological analysis of tissue damage is used to determine the damage threshold in a penetrating electrode model. When compared with the maximum electric field in a plate electrode model at the defibrillation threshold, we determined that the safety factors, the ratio of the damage and defibrillation thresholds, for 10 ms and 300 ns were very similar. Cross-sectional staining results showed a safety factor of 5.38 for 300 ns shocks and 6.29 for 10 ms shocks, $p=0.22$. When combined with our previous result that

nanosecond shocks can defibrillate at lower energies, nanosecond defibrillation becomes a more viable option for low-energy defibrillation.

The stimulation strength-duration curve for cardiac tissue from 200 ns to 10 ms is presented in Chapter 5. This curve allowed us to predict how defibrillation shocks of any duration will affect the heart and revealed an energy minimum at 100 μs. The curve deviated from that predicted by the RC cell model at shorter pulse durations, with nanosecond shocks stimulating tissue at electric fields that are lower than predicted.

Despite these promising findings, there are hurdles to the implementation of nanosecond defibrillation in clinics and hospitals. The pulsers required to produce such short shocks are typically large and made of many feet of coaxial cables or large capacitor banks. This puts a limitation on portability. Additionally, the high voltages required for nanosecond defibrillation require large power supplies and pose a safety hazard.

It may be possible to overcome these limitations with a recently developed technique called megahertz compression. Pakhomov et al. showed that it is possible to excite and electroporate cells using a pulse train of nanosecond shocks of much lower amplitudes at MHz frequencies [38]. For trains of 5 and 100 shocks of 340 ns duration, the amplitude required for nerve stimulation decreases at pulse repetition frequencies above approximately 5 kHz. For 100, 200, and 400 ns shocks, the stimulation amplitude depends only on the time-averaged amplitude and burst duration. For a burst of 100 shocks of 200 ns duration at 3.3 MHz, the time averaged stimulation threshold is the same as the threshold for a 300 μs shock that is the same duration as the pulse train. In Chapter 6, we show that in cardiac tissue, MHz compression is also effective in reducing the stimulation electric field threshold.

Another point of consideration is the use of even shorter nanosecond defibrillation shocks, since these could potentially defibrillate at even lower energies than longer nanosecond shocks. It has been demonstrated that stimulation of excitable cells is possible with shocks as low as a few nanoseconds. In chromaffin cells, 5 ns shocks are able to stimulate the cells, causing Ca^{2+} entry which triggers catecholamine release [39]. Electroporation plays a role in this process, but stimulation is repeatable after minutes. In nerves, 12 ns stimulation is possible without electroporative damage [27].

In Chapter 7, we investigate 60 ns defibrillation determine whether these shocks are more efficient at terminating fibrillation. The 60 ns stimulation threshold was also determined and used to extend the stimulation strength-duration curve of Chapter 5.

Finally, we investigated 80 ns shocks with a second, negative phase of varying amplitude to determine whether bipolar cancellation occurs. Bipolar cancellation uses short biphasic shocks, where, instead of increasing the cellular response as for longer shocks, the second phase discharges the membrane and results in a lower amplitude response. This modality has been studied in various cell types [40, 41], but not yet in tissues. If this technology is realized on a larger scale, it could result in the replacement of implantable defibrillators and pacemakers with ones external to the body, or allow us to minimize shock effects on tissues for external defibrillation.

CHAPTER 2:

METHODS

2.1 General Approach

2.1.1 Heart Harvest

During rabbit surgeries, we used procedures designed to limit animal discomfort, stress, pain, and injury to the unavoidable minimum. All procedures were approved by the Old Dominion University Institutional Animal Care and Use Committees (IACUC).

Rabbits were anesthetized with 3-5% isoflurane in oxygen first in an induction chamber, and, once non-responsive, through a nose-cone. The rabbits were then heparinized (500 IU/kg) intravenously through the marginal ear vein. A toe pinch on each limb was used to ensure that the animal had reached a surgical plane of anesthesia. A bilateral thoracotomy was performed, with incisions placed laterally up the ribcage and just above the diaphragm. The ribcage was pulled up to expose the heart, which was then excised and placed in cold (4° C) Tyrode's solution.

The aorta was then cannulated and back-perfused with cold Tyrode's solution to arrest the heart. This was done rapidly to ensure that the heart was arrested before is begins to suffer from hypoxia, and to extend the allowable amount of time before the heart is placed in the Langendorff-perfusion setup and re-oxygenated. A small cut was made in the right atrium, and a 3-4 cm long tube was pushed through the mitral valve into the right ventricle to reduce pressure on the heart and prevent build-up of fluid caused by the aorta being tied off.

2.1.2 Langendorff-perfusion

The Langendorff-perfusion life support system allows the heart to stay alive outside of the body for several hours. Langendorff-perfusion refers to the method of retrograde perfusion of the aorta. The aorta was cannulated and perfused with oxygenated Tyrode's solution (in mM: NaCl: 128.2, NaCO3: 20, NaH2PO4: 1.2, MgCl2: 1.1, KCl: 4.7, CaCl2: 1.3, glucose: 11.1). The aortic valve closes under retrograde perfusion, so the solution was forced into the coronary arteries, providing nutrients and oxygen to the heart.

During perfusion, the heart was placed in a chamber and superfused with Tyrode's solution to maintain an ambient temperature of 37.5 ± 1° C. The perfusate was also temperature controlled at the same temperature. Their temperatures were monitored by two thermocouples, one placed in the chamber, and the other placed immediately before the cannula in the tubing supplying Tyrode's solution to the heart. A blood gas mixture (95% O_2, 5% CO_2) was bubbled through the reservoir of Tyrode's solution via an aerator stone to maintain the pH between 7.25-7.45. The warmed, oxygenated Tyrode's solution was pumped to the heart at a variable rate to maintain a pressure of 50-80 mmHg in the heart. The pressure was monitored via a sensor placed in the tubing leading to the cannula.

2.1.3 Optical Mapping

To be able to visualize the electrical signals of the heart, we embedded a voltage-sensitive dye in the cell membrane, excited the fluorophore, and filtered and recorded the resulting emission signal. As shown in Figure 3, a 1000 mW, 671 nm diode laser (Shanghai Dream Lasers) was directed through a 5° conical diffuser to evenly distribute the laser light. The light was then

reflected off of a dichroic mirror with a cutoff wavelength of 690 nm to uniformly illuminate the heart. The fluorescence signal from the heart was then passed through the dichroic mirror and a 715 nm long pass filter to a CCD camera ("Little Joe", SciMeasure, Decatur, GA) where it was recorded at 1000 frames per second.

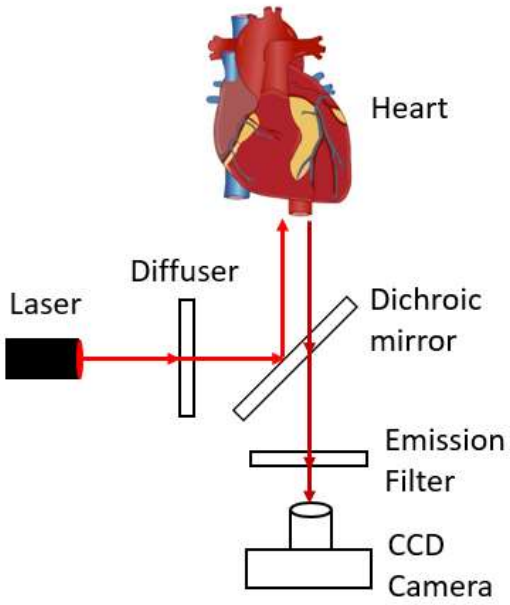

Figure 3. The optical mapping setup used for the Langendorff-perfusion experiments. The heart is stained with Di-4-ANBDQBS, a voltage-sensitive fluorescent probe, which is excited by a diffused laser (671 nm). Fluorescent light is then passed through a long pass filter with a cutoff of 715 nm and recorded by a CCD camera.

During experiments, the near-infrared dye Di-4-ANBDQBS was used to stain the Langendorff-perfused heart. 10 mg of dye was dissolved in 1.2 mL ethanol to form a stock solution, and for each experiment, 20-60 µL of the dye solution was diluted with 10 mL of Tyrode's solution and injected as a bolus through a filter (PVDF Syringe Filter, pore size: 0.22 µm). The filter was used to remove any undissolved dye particles.

After 15 minutes of equilibration in the setup, 30-60 μL of the voltage sensitive dye DI-4-ANBDQBS (stock solution: 10 mg dye in 1.2 mL ethanol) were diluted in 10 mL Tyrode's solution and injected as a bolus. Initial recordings were then taken to capture the spontaneous activity of the heart. 10-15 mM of 2,3-butanedione monoxime were then added to the perfusate to eliminate contractions. Once contractions had ceased, several baseline recordings were captured both of sinus rhythm and the response to a stimulating electrode. The stimulating electrode was a point electrode with a distant ground and was removed before defibrillation shocks were applied. The stimulus duration was 10 ms, at a repetition frequency slightly faster than sinus rhythm, and the voltage amplitude was increased until the heart began responding at the frequency of stimulation. The heart was typically paced at twice the minimum stimulation amplitude.

The dye itself is composed of three parts: the polar head group, the membrane binding motif, and the fluorophore. Di-4 refers to the alkyl/hydrocarbon chains with 4 carbons responsible for membrane binding. ANBDQ (AminoNapthylButydienlyQuinolinium) is the flurophore of the dye, and is responsible for the wavelength range of peak absorption, which in this case is red-shifted from previously synthesized dyes. The polar head group, indicated by the letters BS, renders the dye insoluble in aqueous solution. Thus it must be dissolved in ethanol or dimethyl sulfoxide (DMSO) [42].

Dye molecules imbedded in the cell membrane absorb a photon when their energy matches the energy difference between the ground state and the excited state of the chromophore. Neither state exists at a set energy level, but rather as an energy distribution. Thus, the probability of a photon of a certain wavelength being absorbed falls on a continuous spectrum. At some point

after excitation, the chromophore returns to the ground state and a photon is emitted (fluorescence).

Voltage sensitivity stems from the properties of the dye that result in translocation of a charge from one end of the fluorophore to the other during absorption or emission. Since the dye is bound perpendicularly to the membrane by the polar head group and hydrocarbon chain, the transmembrane voltage will change the amount of energy required to move the charge. This results in a spectral shift proportional to the transmembrane voltage since the energy needed to move a charge along an electric field is proportional to the field [43]. Capturing the resulting fluorescence through a long-pass filter results in a change in the total fluorescence proportional to the change in the transmembrane voltage. This enables us to visualize the excitation patterns on the surface of the heart.

Optical mapping traces were recorded for each shock application, spanning from a few seconds before to a few seconds after the shock. Traces were analyzed for any electrophysiological changes such as baseline shift, action potential duration, and diastolic interval.

2.1.4 Fibrillation Induction

For the 300 ns defibrillation experiments, fibrillation was induced by gently rubbing the leads of a 9V battery on the surface of the heart. After sustained fibrillation (>30 s), defibrillation shocks were applied to the heart. In 8 of 12 animals, fibrillation spontaneously terminated, and 5-10 μM pinacidil was added to the perfusate to shorten the action potential duration (APD) and increase the likelihood of achieving sustained fibrillation.

This method was often not very successful, with an average number of sustained fibrillation events being less than 15 per heart. In order to obtain the maximum amount of data per heart, it was vital to more easily be able to induce fibrillation. Koch et al have induced fibrillation in rabbit hearts using a 50 Hz sinusoidal wave of increasing amplitude, with an average threshold of fibrillation of 215 mA [44]. Based on their work, we built a circuit to apply a 60 Hz current to the heart as shown in Figure 4. Current is applied to the heart through the same plate electrodes used to defibrillate. The fibrillation inducer was connected with banana plugs and was disconnected before applying the defibrillation shock.

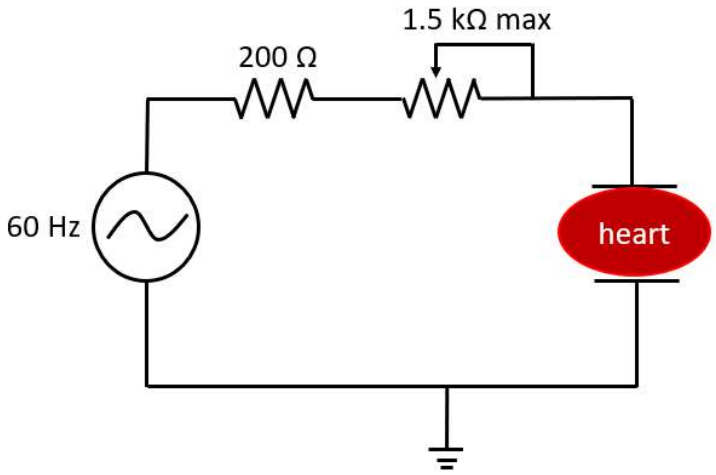

Figure 4. Design for the device used to induce fibrillation. This consists of a high power resistor and a rheostat in series, with a current range of 70-600 mA. The circuit is powered by outlet power, and the current is modified by changing the resistance of the rheostat.

For the MHz compression and 60 ns defibrillation experiments reported in Chapters 6 and 7, the current supply was plugged in, with the rheostat turned to the maximum resistance. The resistance was then gradually reduced until the current through the heart reached 200-300 mA, as

measured using a multimeter placed in series with the entire circuit. This current was then sustained for 5 seconds, after which the current source was unplugged. This method resulted in sustained fibrillation without the use of pinacidil for the majority of the duration of the experiments. Using this method, we were able to induce more than 30 sustained fibrillation episodes per heart (on average). Towards the end of the experiments, it was even possible to induce fibrillation after the heart no longer returned to sinus rhythm when defibrillated, but instead stopped responding entirely.

At the beginning of experiments, approximately 200 mA was required for sustained fibrillation. This value typically increased slowly during the experiment, with about 300 mA required after 2 to 3 hours. We observed that if the heart was exposed to currents above the threshold for fibrillation induction (e.g. by 10-50 mA) the threshold increased by the excess amount of the current, i.e. subsequent induction of fibrillation required at least as much current as was applied in the previous induction.

2.1.5 Determining defibrillation thresholds

Rabbit hearts were harvested and placed in a Langendorff-perfusion optical mapping setup as described above. Hearts were injected with a bolus of voltage-sensitive dye, which allowed the visualization and recording of excitation signals. Fibrillation was induced according to the above protocol. Once fibrillation was sustained for 30 seconds, a defibrillation shock was applied via two angled plate electrodes contacting both sides of the heart. If defibrillation was successful, fibrillation was be induced after one or two minutes of recovery. If defibrillation was not successful, the shock voltage was increased and a new shock is applied, until the heart was

successfully defibrillated. If the heart spontaneously stopped fibrillating, we re-induced fibrillation.

For each experiment, one pulse condition was randomly selected for the first threshold determination. The remaining conditions were randomly selected from until all conditions were tested. Once all thresholds were determined, we repeated the whole procedure and determined the thresholds again, to assess the reproducibility of the threshold determination. We observed some variation in the defibrillation thresholds, which could be due to the fact that fibrillation is a complex process and the success of a defibrillation shock depends to some extent of the particular configuration of activation fronts at the time the shock is delivered. Variation could also occur simply because the heart slowly deteriorated during the repeated application of fibrillation induction currents and defibrillation shocks. If we observed a variation of more than 20% between the initially measured threshold and the subsequently re-measured thresholds, we concluded that the heart had deteriorated to an unacceptable degree and discarded the results.

If the initial shock successfully defibrillated, we decreased the voltage. If defibrillation was not successful, voltage was increased. Both increases and decreases were done in steps of approximately 100 V at the pulser. The 47 Ω resistor placed in series for impedance matching for most experiments attenuated the signal by approximately 80%, resulting in voltage steps of around 20 V, or 5-10 V/cm. 300 ns defibrillation required a 13.7 Ω resistor in series, while no resistor was for 60 ns defibrillation and stimulation. Approximately 5-10 steps were required to determine each threshold.

Both voltage and current waveforms were recorded, as well as optical mapping traces spanning a few seconds before defibrillation to several seconds after. The frame recorded concurrent with

shock application was marked by amplifying the trigger output of the oscilloscope to act as a TTL signal for the software to recognize that a shock had been applied.

Current and voltage recordings were used to calculate the energy of the defibrillation shocks. For Chapter 6, the average threshold was determined by analyzing one duty cycle at the beginning of the pulse train. The average voltage as a percentage of the maximum for this duty cycle was then applied to the threshold electric field.

For each heart, the threshold is the minimum voltage at which defibrillation was achieved. However, the probability of defibrillation success does not abruptly go from 0% to 100%, but typically follows an extended sigmoidal curve, both in individual hearts and between individuals. The electric field approximation (voltage divided by electrode spacing) as well as the binary yes/no of defibrillation success are compiled to yield the defibrillation success curve for each shock condition. This data is fitted with a sigmoidal curve, the inflection point of which is the 50% effective dose value (ED50). This number is compared between pulse conditions.

2.1.6 Energy Calculations

The voltage and current waveforms recorded for each shock application are used to calculate the deposited energy. The waveforms are multiplied at each point to give the power curve, which is then integrated over time to give the energy.

In the case of longer shocks as well as the pulse trains used in Chapter 6, further calculations were required since the Pearson probe used to measure the current has a droop rate of 0.03% / μs, which means it can only monitor the current during the initial part of our pulse train. In these

instances, only the first 10 μs of the waveform were used to calculate the average power, which was then multiplied by the total shock duration to give the energy. This process was repeated for the positive and negative phases for biphasic shocks.

2.1.7 TTC / PI Staining and Sectioning

Histological assessments can be useful for analyzing tissue death or electroporation. Propidium iodide can enter cells with permeabilized membranes (but not those with intact membranes). After entering the cell, the dye binds to DNA or RNA and becomes strongly fluorescent. It should be noted that membranes with pores smaller than approximately 1.5 nm are impermeable to PI, but permeable to smaller ions [32], and nanosecond shocks have been shown to create pores as small as 1 nm.

Triphenyltetrazolium chloride stains metabolically active tissue red when it is reduced by dehydrogenases in the presence of the metabolic byproduct NADH. These byproducts are washed out of damaged cells, and thus, these regions are unstained. [45]

For experiments characterizing the electroporative damage of 300 ns defibrillation, a single shock was applied to hearts, which had been perfused with PI (10 mg/mL, Sigma Aldrich) diluted in Tyrode's solution (30 μM total) for 5 minutes, after the shock, PI perfusion continued for a further 5 minutes. The continuous perfusion ensured that even transient permeabilization of the membrane allowed PI entry and staining. Control hearts were injected with 50 μL Triton X-100 (5%) during PI perfusion. After 10 minutes of PI perfusion, the hearts were perfused with fresh Tyrode's solution for 20 minutes to wash out excess PI.

To facilitate sectioning, all hearts were partially frozen (30 minutes at -20°C), sectioned into ~2 mm slices, and immersed in TTC (30 mM in 0.9% saline) for 20 minutes in an incubator (37°C).

Sections were then imaged with a Canon EOS 6 Mark II camera for TTC staining and an Olympus SZX16 microscope with a FITC cube to quantify PI fluorescence. Fluorescence images were captured using a Hamamatsu C9100 EM-CCD camera in conjunction with the HCImageLive software, version 4.4.0.11.

During experiments determining the safety factor of 300 ns defibrillation, treated hearts were perfused with propidium iodide (PI) (10 mg/mL, Sigma Aldrich) diluted in Tyrode's solution (30 μM) for the entirety of the experiment. After five minutes of equilibration to allow the heart to stabilize in the setup, treatments were performed, lasting no more than 15 minutes. After treatment, PI perfusion continued for 30 minutes to ensure that post-shock perfusion for both the first and last lesions was similar and any post-shock cell death was captured. The hearts were flushed with cold (0°C) Tyrode's solution to arrest the heart and flush out any remaining PI. The hearts were then placed in formalin for at least 30 minutes to fix the tissue.

Fluorescence images of the surface of the heart were captured at each shock application site. Additionally, each individual lesion was excised using a scalpel with a minimum border of 1 mm undamaged tissue in all directions, and a longitudinal cross section of the lesion, intersecting both electrode points of insertion and perpendicular to the myocardial surface, was imaged. In some cases, when the tissue was not adequately sectioned along the midplane of the electrodes, a further, transverse cut was performed at each electrode insertion point, and the resulting surface was then imaged.

2.2 Nanosecond Pulse Generation

Rectangular pulse generators come in several different forms, but follow the same basic principles. For low voltage, longer duration applications, it is often sufficient to use a direct current power supply with a switching mechanism to control the duration of time the pulse is "on". However, for higher voltage (kilovolts), short (sub-millisecond) duration, switching capabilities are limited. Thus, charge is typically stored over a longer period of time in a capacitor or inductor and then discharged as a square pulse via a high voltage switch such as a spark gap. Such pulse-forming networks often take the form of capacitor banks or transmission lines, which can be viewed as extended cylindrical capacitors.

When using capacitor banks, multiple switches are required, however, transmission line pulse generators require only one switch and easily obtainable coaxial transmission line cables. A drawback of this design is that typically long cables must be used, though for shorter pulse durations, this becomes less of an issue. Additionally, the pulser must be impedance matched with the load to avoid reflections. Finally, a simple charged transmission line pulser with the power supply connected at one end and the load connected (via spark gap) at the other has the limitation of only being able to apply half the voltage supply to the load. However this configuration is simple in its construction and was selected for both the 300 ns (fabricated by the pulsed power lab) and 60 ns (design and fabrication detailed below).

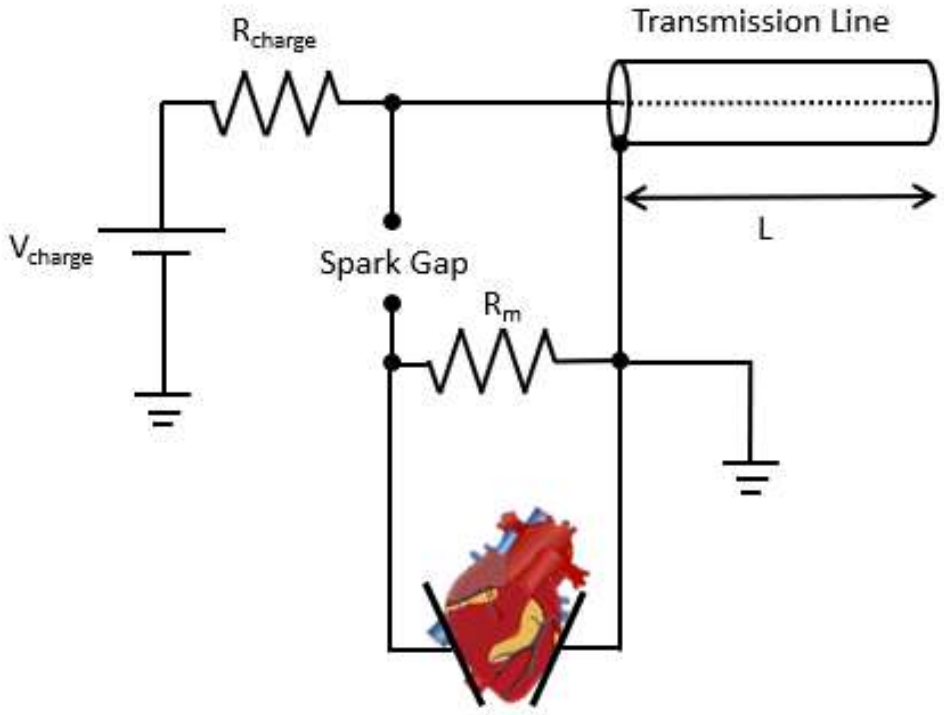

Figure 5. Transmission line pulse generator design used for 300 ns and 60 ns defibrillation. The transmission line is charged through a charging resistor using a high voltage power supply. Once the charge voltage reaches the breakdown voltage of the spark gap, the circuit is closed and the transmission lines deposit the stored charge into the heart.

For a transmission line pulse generator, the pulse duration (*d*) depends on the length of the transmission line (*l*) and the speed of light in the transmission line (*v*).

$$d = \frac{2l}{v} \qquad \text{Equation 2}$$

In our case, the desired pulse duration is 60 ns and v = 0.66c, where *c* is the speed of light in vacuum. Thus, the desired cable length is 5.94 m or 19.5 ft.

When designing a nanosecond pulser, it is important to ensure impedance matching between the pulser and the load. The coefficient of reflection is:

$$\Gamma_{pl} = \frac{Z_p - Z_l}{Z_p + Z_l} \qquad \text{Equation 3}$$

Where Γ_{pl} is the reflection coefficient, Z_p is the pulser impedance, and Z_l is the load impedance. The impedance of the load does not match the impedance of the pulser, the reflection coefficient is non-zero, and a portion of the signal is reflected, attenuating the signal amplitude at the load and resulting in oscillations in the pulse shape recorded at the oscilloscope. So to achieve zero reflection, the load impedance and the pulser impedance should be as similar as possible.

2.1.1 Nanosecond pulsers

For the 300 ns defibrillation experiments described in Chapter 3, a transmission line pulse generator was used. The pulser consists of seven parallel coaxial cables (RG-217U) which are used as a capacitor (21.2 nF) and are charged with a high voltage power supply and discharged through a spark gap. To achieve better impedance matching, a 13.7 Ω resistor is placed in parallel with the heart.

For safety factor experiments and determination of the stimulation strength-duration curve (Chapters 4 and 5), nanosecond shocks were delivered using the Pulse TX generator from Pulse Biosciences (Hayward, CA). The generator is capable of supplying shocks of amplitudes from 2 to 15 kV with durations varying from 200 ns to 1 μs.

For MHz compression experiments (Chapter 6), nanosecond pulse trains of 1000, 1000 ns shocks at 0.4 Hz were generated using a custom-made pulse generator consisting of a capacitor bank

charged by a DC power supply (Kepco Power Supply Model APH 1000M). The pulse was shaped by a digital delay/pulse generator (Directed Energy PDG-2510).

The design and fabrication of the 60 ns pulser used in Chapter 7 is described in Section 7.2.1.

Voltage waveforms were captured using the internal PulseTX oscilloscope and a Teledyne Lecroy Wavesurfer 10M oscilloscope.

2.2.2 Detecting Placement of ns shocks

For experiments using the 300 ns transmission line pulse generator, an induction loop was used to send a trigger signal to the software to mark the lower right corner of the acquisition frame during which the shock was applied. The loop was placed near the spark gap, and when the accumulated charge arced, a current was induced in the induction loop. This current was detected by an acquisition board (BNC-2110, National Instruments).

For experiments using pulse generators consisting of enclosed capacitor banks, using an induction loop was not possible. Instead, a voltage probe was used to detect the voltage at the electrodes, which was then recorded by an oscilloscope. The oscilloscope has a trigger out signal that supplies a 100 ns, 5 V pulse, which is too fast to detect with the acquisition board.

To extend this pulse duration to that of a usable transistor-transistor logic (TTL) signal on the order of a few milliseconds, a buffer amplifier was used. The circuit design used to accomplish this is shown in Figure 6. For the integrated timing circuit (NTE955M, NTE Electronics), the amplitude of the output pulse is determined by Vcc, and the duration is determined by $t = \ln(3) \cdot RC$. For Vcc = 5 V, the trigger threshold is 1.67 V, which will allow the circuit to be

reliably triggered by the oscilloscope output, and the output amplitude will be able to trigger the acquisition board. To achieve a pulse duration of approximately 7.5 ms, 10 μF and 680 Ω are selected for C and R. C_D is a decoupling capacitor used to shunt electrical noise, and a 33 nF capacitor is used.

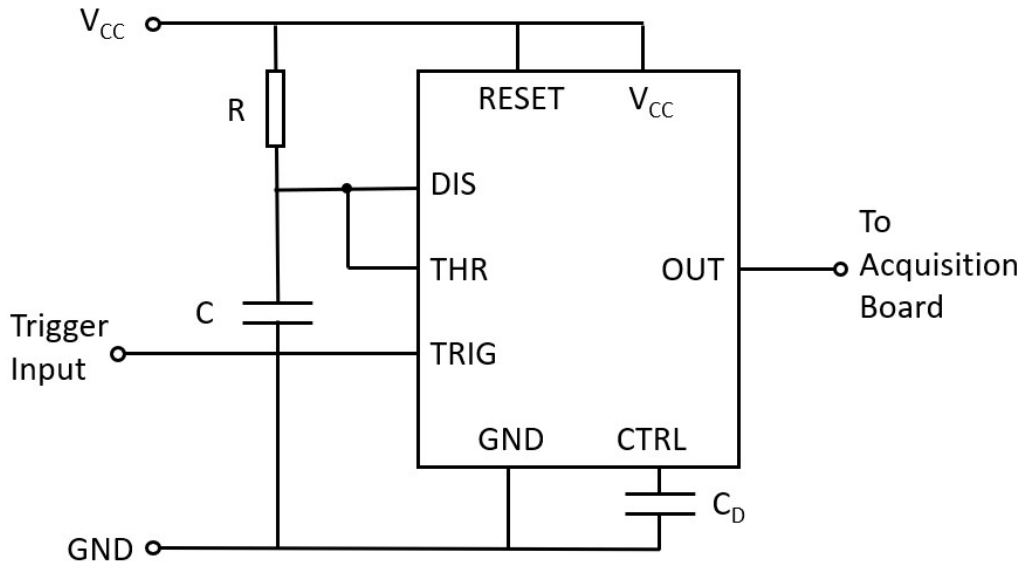

Figure 6. A buffer amplifier used to increase the signal duration when triggered from the oscilloscope. The input trigger was a 5 V, 100 ns pulse from the oscilloscope that had detected a voltage waveform. C and R were selected such that the output pulse duration is at least 5 ms in duration. V_{CC}, the supply voltage, was selected to be 5 V, resulting in a trigger threshold of 1.67 V, and C_D was used to shunt electrical noise.

Thus, the trigger out signal from the oscilloscope was passed through the timing circuit to increase the duration and sent to the acquisition board, where it was detected, and used to place a marker in the optical mapping recording to indicate the shock placement.

2.3 Millisecond shock generation

For the defibrillation experiments detailed in Chapter 3, we used a house-made resistor-capacitor circuit, with the capacitors connected to the plate electrodes via solid state relays. Two capacitors (10 mF each) were connected in parallel and connected to a power supply via a charging resistor. The power supply was set to the desired maximum voltage, and the capacitors were discharged through the heart when the solid state relays were closed for a total duration of 10 ms.

For the experiments in Chapters 4, 5, 6, and 7, the same pulse generator as for MHz compression was used. The pulser is capable of producing monophasic and biphasic waveforms based on the input trigger signals supplied by the digital delay/pulse generator (Directed Energy PDG-2510). The pulse duration ranges from 1-10,000 μs, with a maximum amplitude of 1 kV. Sample monophasic and biphasic waveforms are shown below.

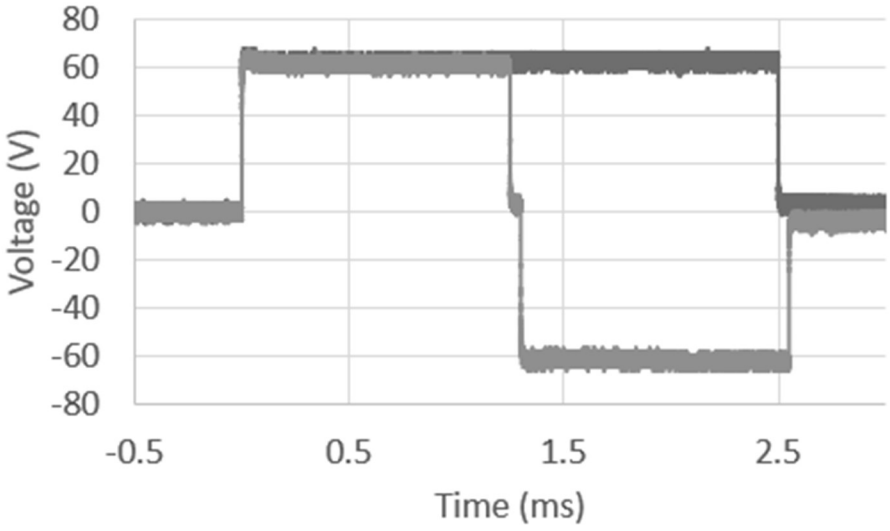

Figure 7. Sample monophasic and biphasic waveforms generated by the custom pulser also used to generate MHz pulse trains.

2.3.1 Timing of stimulation shocks

For stimulation experiments, the heart is paced with 10 ms shocks at a frequency slightly faster than sinus rhythm (3-6 Hz). One millisecond shock is then replaced with the test condition shock of a different pulse duration. Particularly in the nanosecond range, this test shock has a high enough amplitude that it could damage the millisecond pulser used for other experiments. Thus, a circuit implementing an electro-mechanical switch was designed to decouple the millisecond pacing shock generation from the test shock generation, see Figure 8.

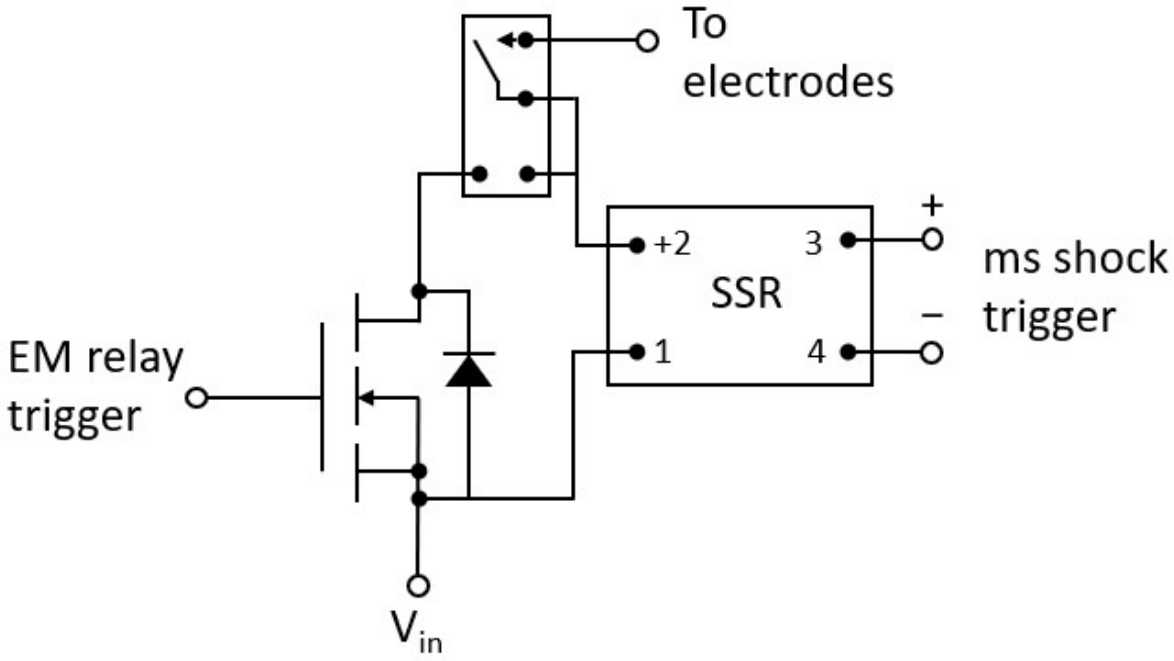

Figure 8. The electromechanical relay circuit, used to shape the millisecond shocks, and decouple the system during application of nanosecond test shocks. V_{in} is used for the voltage of the millisecond pacing shocks as well as to power the MOSFET. When the trigger signal is sent to the MOSFET, the electromechanical relay is closed. A second trigger signal is then used to close the solid state relay to

deliver a millisecond pacing shock to the heart. The end of the ms shock trigger signal ends the millisecond pulse. After this, the relay trigger signal goes to low and the EM switch is opened.

A 5 V TTL signal is sent to an n-channel MOSFET (IRL640, Vishay Electronics). The electromechanical relay (G5Q-1A4-EL2-HA-DC12, Omron Electronics) requires a switching voltage of 12 V, while the acquisition board can only output a 5 V signal, so the MOSFET switches on the connection to a higher voltage source. The electromechanical relay then closes and connects the millisecond shock circuit to the electrodes at the heart. 30 ms after the relay is closed, the millisecond shock is applied, and after a further 5 ms, the relay is opened to disconnect the millisecond pulser from the electrodes. After 5 millisecond shocks have been applied, the relay remains open while the nanosecond shock is applied, after which the switching process resumes as before until the end of the optical mapping recording. See Figure 9 for a timing chart.

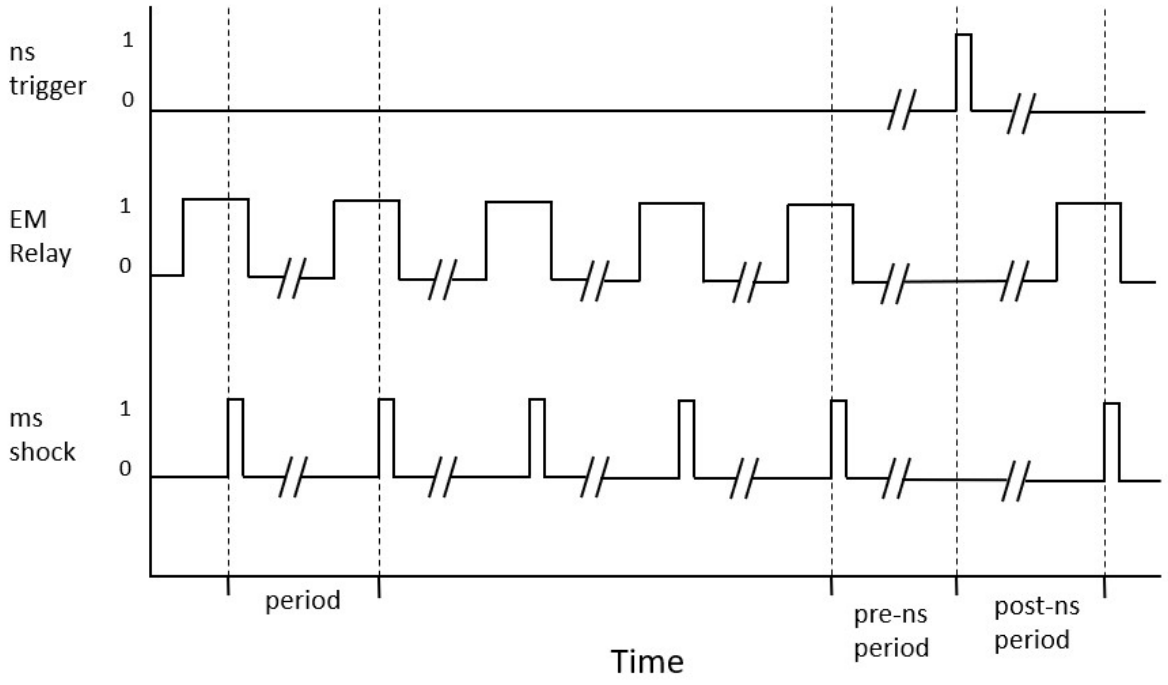

Figure 9. Timing chart for the various relays and trigger signals. When the EM Relay signal is high, the relay is closed and the millisecond shock circuit is connected to the heart. The millisecond shock relay signal then shapes the millisecond shock, after which the EM relay opens. After 5 millisecond shocks, the relay remains open to decouple the millisecond shock delivery circuit during the application of a single test shock.

The period between the millisecond pacing shocks is set to be slightly shorter than for sinus rhythm, usually 200-300 ms. The pre- and post- nanosecond shock periods are also variable, but are typically set to the same value.

The millisecond shock is shaped using a solid state relay (SSRDC100DC40, Omega Engineering) with a digital trigger from the acquisition board. The shock is passed through the EM relay to the electrodes.

To trigger the nanosecond shock, a TTL signal is sent from the acquisition board to the external trigger of the delay generator, which then sends a signal to the custom pulse generator also used for the MHz compression experiments, or to the Pulse Biosciences pulser (see Section 2.2).

2.4 Electrode Configurations

2.4.1 Plate electrodes

The electrodes used for delivering defibrillation shocks are composed of two aluminum plates with a thickness of 1 mm. For the 300 ns defibrillation experiments, the lateral dimensions are 1.5 x 3 cm. The electrodes were designed to form a 30° angle at the apex, to follow the shape of the ventricles and maximize the intracardial field (see Figure 10).

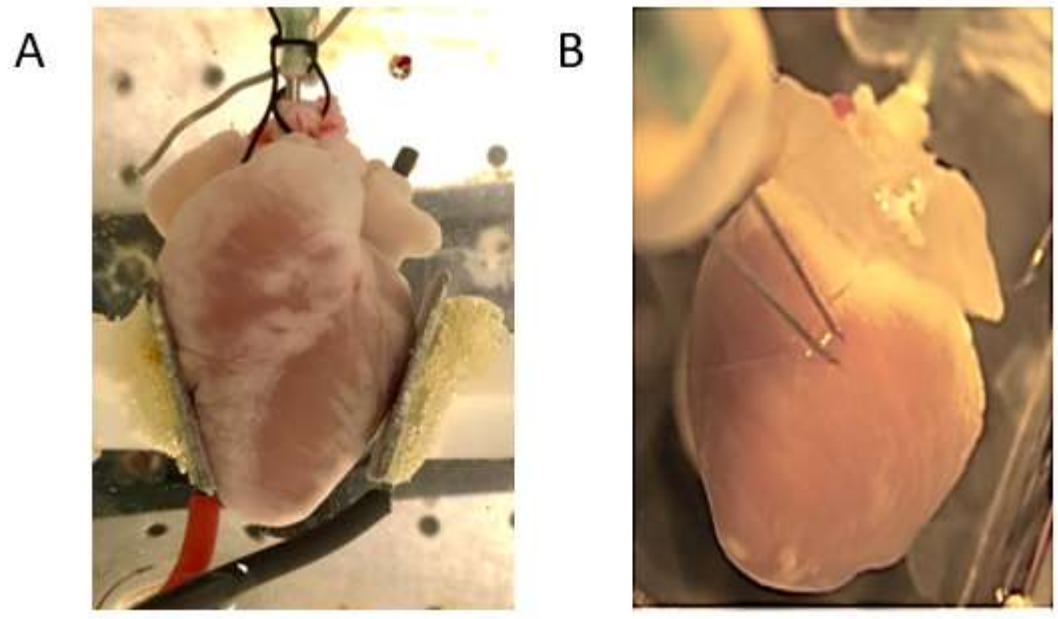

Figure 10. Electrode configurations. A) The angled plate electrodes used in later defibrillation experiments. B) The needle electrodes used in Chapter 4.

In all other experiments, the electrode size was changed to 2 x 2.5 cm, to maximize the surface area of the electrodes making contact with the heart while minimizing overhang.

2.4.2 Needle Electrodes

For the safety factor experiments, two parallel 250 μm tungsten needles were inserted into the epicardium. The electrode spacing was 4 mm, and the electrodes were insulated with a hemisphere of silicone with the terminal 4 mm exposed. To mark the insertion points, the electrode tips were dipped into surgical ink before being inserted into the epicardium. Electrode insertion points were at least 1 cm apart, and placed on both the posterior and anterior walls of both ventricles, allowing for up to 18 applications per heart.

2.5 Mathematical model of nsPEF electric field

To compute the static electric field distribution in the parallel plate electrode geometry that we used in prior defibrillation experiments, a spherical shell (12 mm inner radius, 15 mm outer radius) of cardiac tissue was modeled in between two perfect conductors of dimensions 30 mm x 30 mm x 2 mm as shown in Figure 11. One plate was set to +V/2 and the other to -V/2, where V is the desired potential difference between the two. The electrodes and the heart were immersed in a solution with the same electrical properties as the Tyrode's solution used in our experiments.

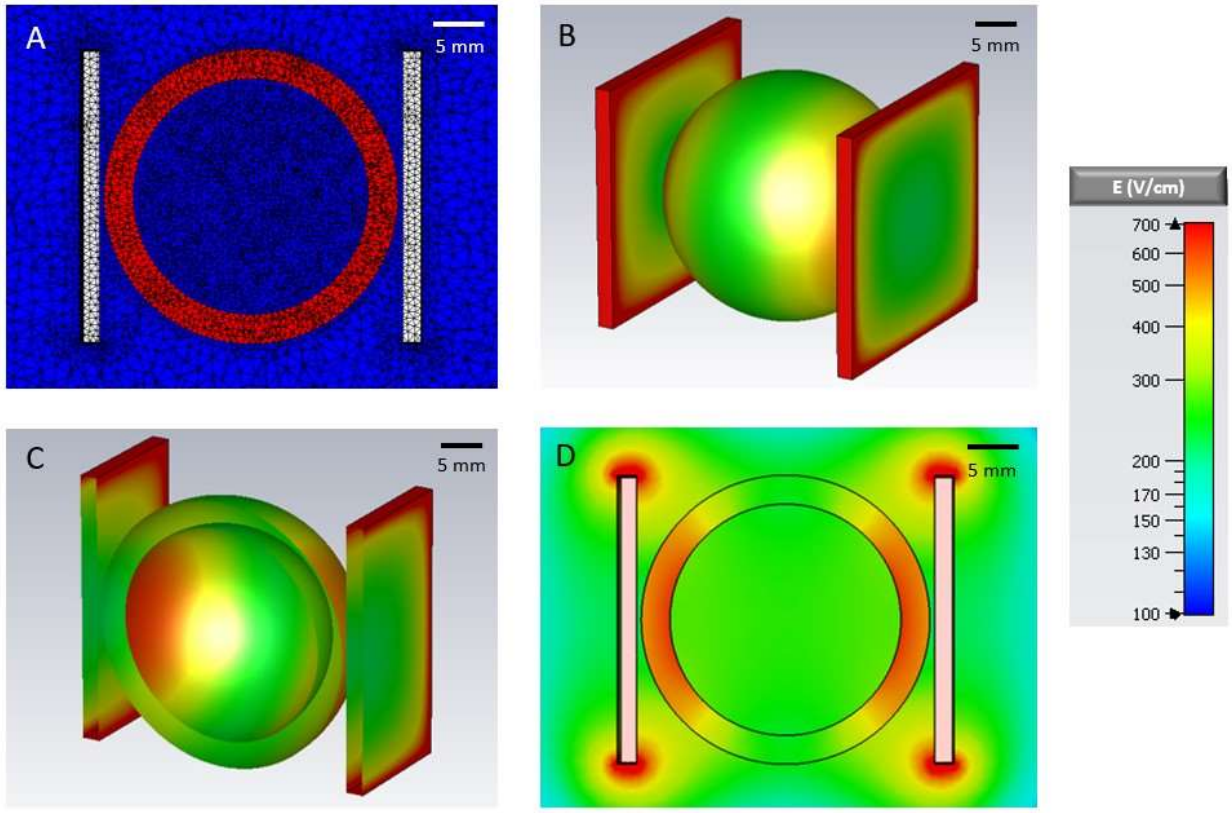

Figure 11. Electric field distribution for a voltage of 1 kV applied to two parallel plate electrodes (separation 2.8 cm) positioned on either side of a simplified heart model. A) 2D mesh view of the xz-plane B) 3D view of the closed cardiac shell model C) The model cut open along the xz-plane and D) 2D view of the xz-plane. The highest field strength is observed at the inner surface of the cardiac shell closest to the electrodes.

In the penetrating electrode configuration (see Figure 12), the electrodes were modeled using two rods of 0.12 mm radius, with a 4 mm separation. The rods penetrated the spherical shell to a depth of 3 mm and were modeled as perfect electrical conductors. A dielectric hemisphere of 5 mm radius was also placed surrounding the sections of needle not inserted into the heart to model the silicone used to insulate and keep the needles in place. One needle was set to +V/2 and the other to -V/2, where V was the desired potential difference between the two.

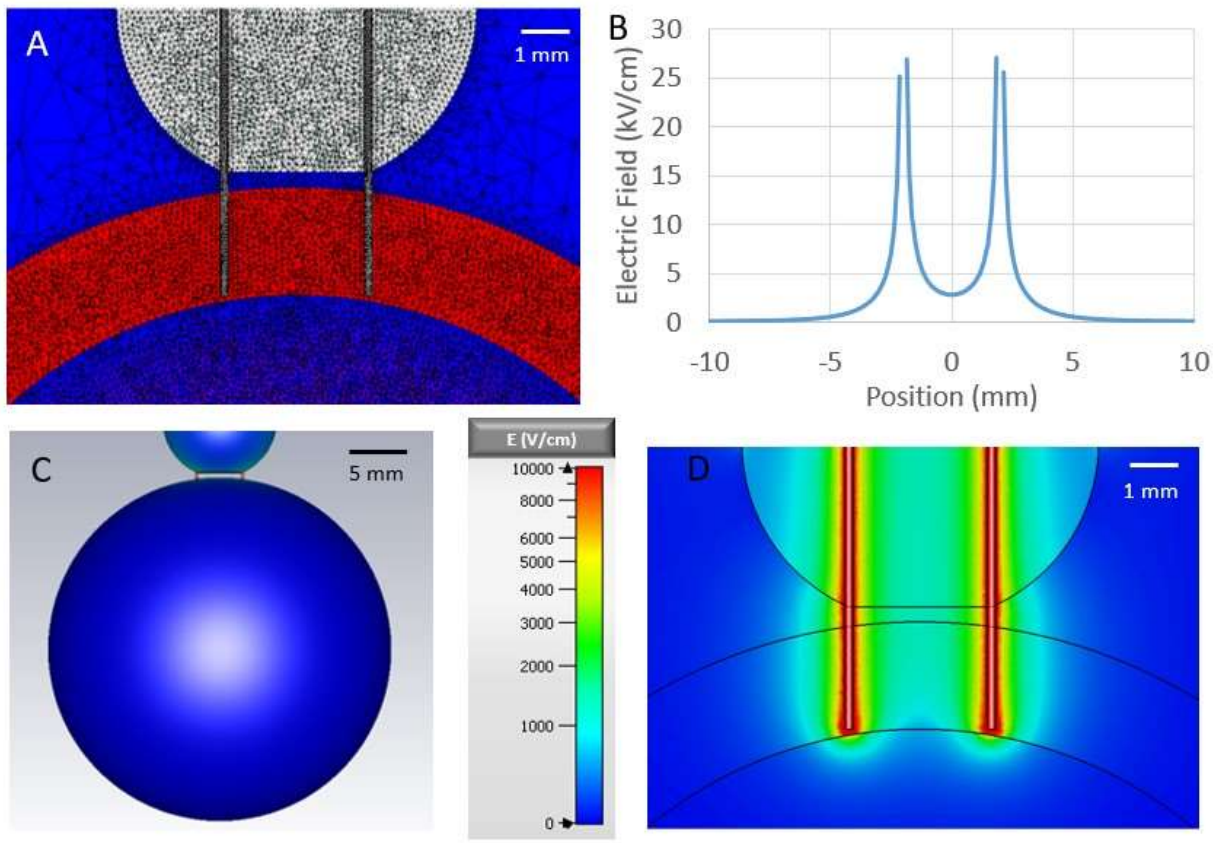

Figure 12. Electric field distribution for 1 kV applied to two needle electrodes inserted into the cardiac tissue of our simplified heart model. A) 2D mesh view of the cross section through the needle electrodes B) field strength along the line perpendicular to the long axes of the electrodes, at a tissue depth of 1.5 mm halfway between the electrodes C) 3D view of the cardiac surface and D) cross-section through needle electrodes.

We used the Computer Simulation Technology (CST) Microwave Studio® 3D Electromagnetic simulation software, specifically the electrostatic solver with tetrahedral meshing to model our system. The solver uses the finite element integration to discretize Laplace's equation, $\nabla \cdot \sigma \nabla V = 0$, where V is the electric potential and σ is the conductivity. We can neglect any permittivity

effects since the dielectric relaxation time constant is much shorter than our pulse duration. The relaxation time is given by

$$\tau_D = \frac{\varepsilon_0 \varepsilon_r}{\sigma} \qquad \text{Equation 4}$$

where ε_0 is the vacuum permittivity and ε_R is the relative permittivity of the material, leading to $\tau_D \approx$ 15 ns for a 300 ns pulse [46]. While conductivity generally depends on frequency, we approximated the conductivity of Tyrode's solution as σ_T = 1.59 S/m [47] and the conductivity of cardiac tissue as σ_C = 0.6 S/m [46]. Note that the solution of the Laplace equation only depends on the ratio σ_T/σ_C, so variations in σ_T or σ_C do not affect our solution as long as they have the same frequency dependency.

Figure 11A shows the tetrahedral mesh of the parallel plate configuration. It can be seen that the mesh is adaptive; in areas with larger variability in the material properties it is finer, and in areas with lower variability it is coarser. The edge length varies from 0.02 to 4 mm, and the total number of tetrahedrons exceeds 1,000,000 in all cases.

The electric field distributions for the parallel plate configuration are shown in Figure 11B-D. The maximum field strength ($E_{max,DV}$) for the ED50 defibrillation voltage (DV) for the parallel plate configuration occurs on the inner surface of the cardiac sphere closest to the electrodes (the enhancement of the electric field at the edges of the electrodes does not extend to the cardiac shell). The relationship between the applied voltage and $E_{max,DV}$ is linear, and the proportionality factor between the applied voltage and the corresponding electric field turns out to be 0.63 /cm.

Figure 12 shows the field distribution in our needle electrode model. Panel A shows the mesh which now includes the needle electrodes and an electrode holder close to the cardiac surface

(see also panel B). Figure 12C and D show the field distribution in the plane defined by the needle electrodes. Note that the field strength increases sharply towards the electrodes, so that for any applied voltage, the different regions of the tissue are exposed to a broad range of electric field strengths. We generally express the strength of electric fields in units of the $E_{max,DV}$, the maximum field that any part of the heart experiences when 1 DV shock is applied in the parallel electrode configuration (see above). Since electric field distributions in both geometries are governed by the linear Laplace equation, the field strength at any point in the heart is linear with respect to the applied voltage: For example, if a 2 DV shock is applied in the parallel electrode configuration, the maximum field strength occurring anywhere in the heart is 2 $E_{max,DV}$.

CHAPTER 3:

300 NS DEFIBRILLATION

3.1 Introduction

The first experiments performed were to determine whether 300 ns shocks could stimulate and defibrillate cardiac tissue. The defibrillation threshold was determined for 12 hearts, and the stimulation threshold was determined for 9 hearts. In two hearts, the defibrillation thresholds for both 300 ns and 10 ms shocks were determined, and the voltage and current waveforms were used to calculate the deposited energy. To see if the nanosecond shocks caused any damage, optical mapping traces were analyzed for abnormalities in the action potential duration and diastolic interval as baseline shift. Additionally, in 6 hearts, a single nanosecond shock with an amplitude high enough for consistent defibrillation success was applied to the heart. Staining with TTC and PI was performed to detect any evidence of electroporation or tissue death.

3.2 Results

We have shown that it is possible to defibrillate with 300 ns shocks at much lower energies than for monophasic 10 ms shocks [48]. Langendorff-perfused New Zealand white rabbit hearts were placed between two plate aluminum electrodes. Fibrillation was induced using a 9V battery rubbed on the surface of the heart. Once sustained fibrillation was induced (>30s), 300 ns or 10 ms shocks were applied through the plate electrodes. If defibrillation was unsuccessful, the voltage was increased and a second shock was applied. The resulting success curve for 300 ns is

shown in Figure 13B. The ED50 defibrillation voltage is approximately 2.35 kV, with an electrode spacing of 3 cm.

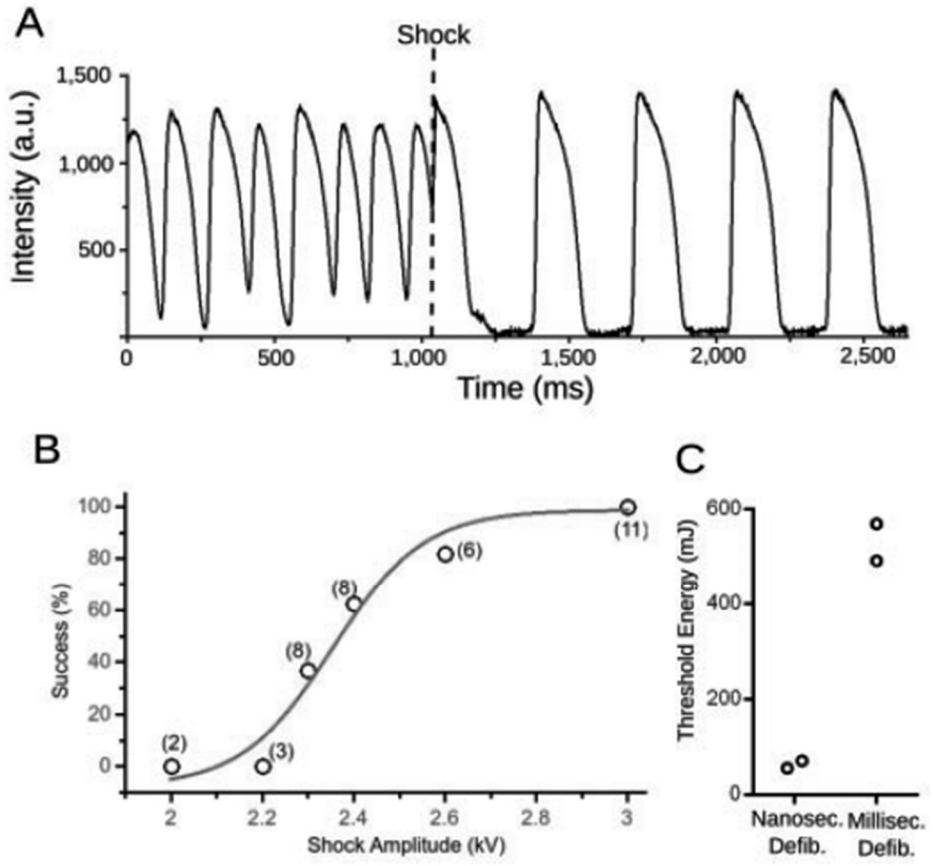

Figure 13. Defibrillation with nanosecond shock (12 hearts). A) Optical recording from a representative surface location on the cardiac surface. The heart is initially fibrillating, before a single shock is applied at the time marked with a dashed line. After the shock, sinus rhythm is restored. B) Defibrillation success rate as a function of shock amplitude. Numbers in parentheses indicate how many observations contributed to each of the data points. The red line shows a sigmoidal function fitted to the data. C) Comparison of defibrillation for millisecond defibrillation (monophasic) and nanosecond defibrillation. Black empty circles indicate the threshold energies that were determined in individual hearts.

3.2.1 Stimulation

Rabbit hearts were consistently stimulated with nanosecond shocks of amplitude 400 V/cm. The resulting action potential shape and duration are identical to those of sinus beats (see Figure 14A). However, the activation clearly originates at the electrodes and activates to whole epicardium within 10 ms as shown in Figure 14B and C. Five hearts were used to determine the success curve for stimulation (Figure 14D). The 50% effective dose threshold (ED50) is approximately 300 V/cm.

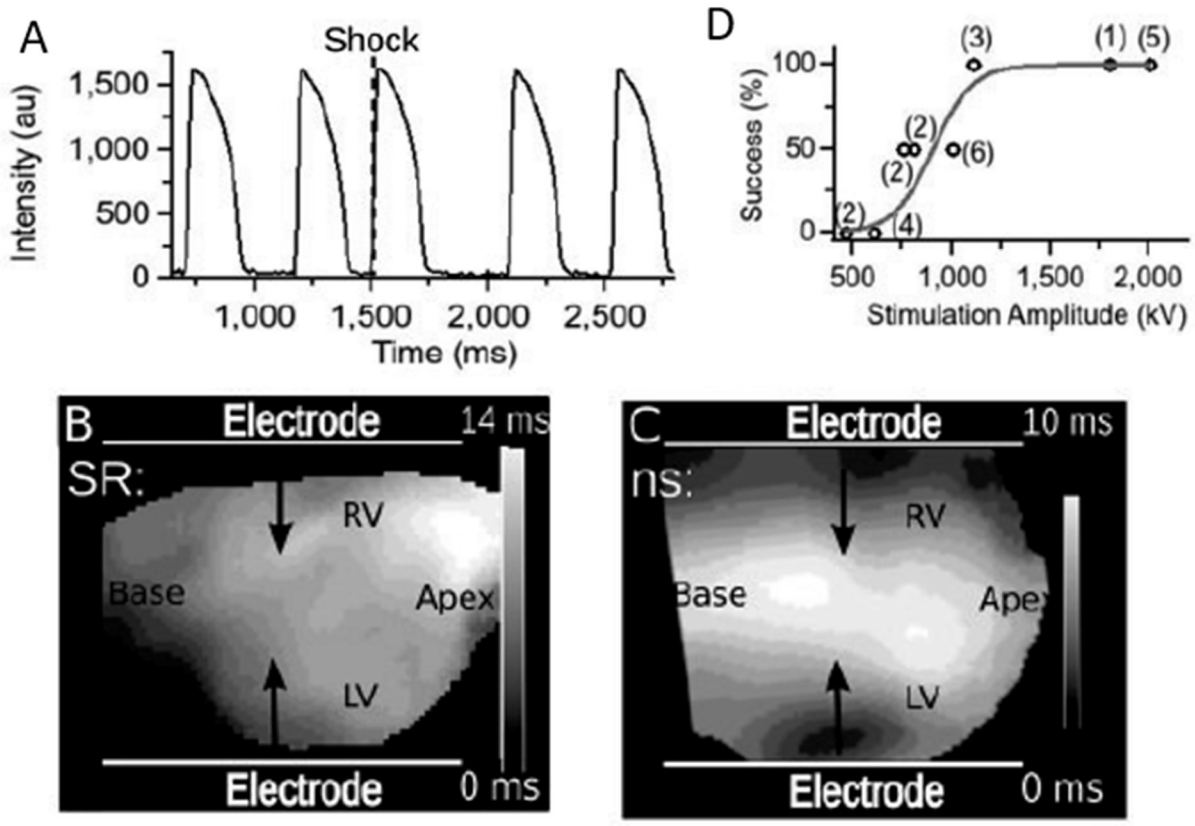

Figure 14. Stimulation of cardiac tissue with nanosecond shocks in 5 hearts. A) Optical mapping recording from a representative location on the cardiac surface. The heart is in sinus rhythm when a single shock is applied at the time marked with a dashed line. After the shock-induced action potential, sinus rhythm continues. B) Activation map for sinus activation. Lighter regions are activated before darker regions. C) Activation map following nanosecond shock activation. D) Stimulation success rate as a function of stimulus amplitude. Numbers in parentheses indicate how many observations contributed to each of the data points.

The stimulation threshold for 10 ms shocks was also determined in the same hearts. The ratio of the defibrillation to stimulation thresholds is 2.6 for nanosecond defibrillation (780 V/cm divided by 300 V/cm) and 4.8 for millisecond defibrillation (12 V/cm divided by 2.5 V/cm).

3.2.2 Defibrillation Energy

In two hearts, the defibrillation threshold was determined for both 300 ns and 10 ms shocks, resulting in a defibrillation threshold of 2.3 kV ± 0.2 kV and 37± 2 V, respectively. For 300 ns shocks, the deposited energy was calculated by measuring the capacitance of the pulser (21.2 nF) and using the following equation, where V is the peak voltage of the pulse.

$$E = \frac{1}{2}CV^2 \qquad \text{Equation 5}$$

This resulted in a defibrillation energy of 64 ± 4 mJ. For millisecond shocks, the current and voltage waveforms were recorded. The energy was then calculated by multiplying the two waveforms to give the power and integrating over the entire pulse. This resulted in an energy of 530 ± 35 mJ, more than 8-fold higher than for nanosecond defibrillation.

3.2.3 Staining

In 6 hearts, a single 300 ns shock of 3 kV was applied, which had 100% defibrillation success in earlier experiments. For a positive control, two hearts were injected with 5% Triton X-100, a surfactant that is toxic to cells and tissues. All hearts were sectioned and analyzed after TTC and PI staining to determine whether tissue death or electroporation had occurred.

Results from one heart can be seen in Figure 15. All other shocked hearts also exhibited uniform TTC staining and no PI staining. Thus, defibrillation-strength 300 ns shocks cause no detectable tissue death or electroporation to the extent that PI can enter the cells. Additionally, since hearts were continuously perfused with PI, this indicates no transient electroporation.

The positive control of Triton X-100 injection shows uniform TTC staining except at the injection site, and no PI fluorescence except at the injection site.

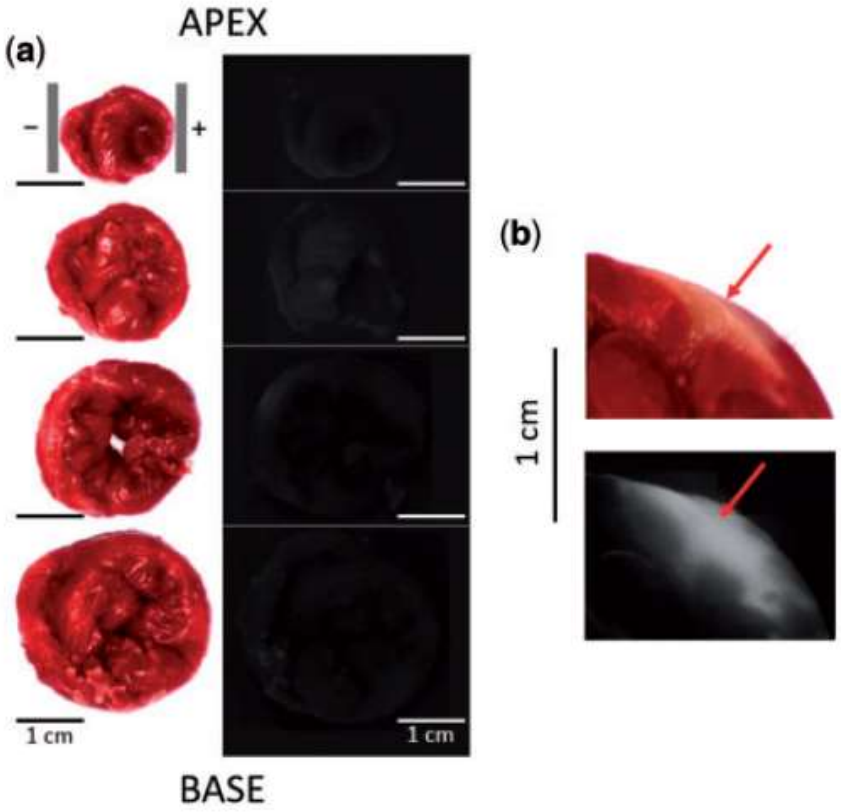

Figure 15. Histological assessment of tissue damage after a single 300 ns, 3 kV shocks. A) Side-by-side view of PI fluorescence (right) and TTC staining (left) for a series of section of the heart arranged from base (bottom) to apex (top). The grey vertical bars in the top left panel indicate the electrode positions. PI fluorescence is so weak that the cardiac tissue is hardly discernable. All images are oriented with the left ventricle on the right side of the image. B) Positive control using an injection of 50 µL Triton X-100. The injection site is marked with a red arrow in both the TTC stain (top) and the PI fluorescence image (bottom).

3.2.4 Electrophysiological effects of 300 ns defibrillation

While histological analysis showed no adverse effects of 300 ns defibrillation-strength shocks, it is possible that the electrophysiological properties of the heart may have been affected. Thus, optical mapping traces were analyzed for any sign of electroporation or other adverse side effects. Electroporation can be detected in optical mapping traces as a baseline shift that can last seconds or minutes due to sustained depolarization. All successful defibrillation recordings were analyzed, but no evidence of baseline shift was found.

Additionally, the diastolic intervals before and after stimulation with nanosecond shocks as well as the action potential duration were analyzed. Comparing the action potential duration of a sinus beat with a subsequent nanosecond shock inducted beat in four hearts (four episodes total) results in a change of 0.2149 ± 2.3%. This is within expected normal variation between sinus beats which showed a variability of -0.523 ± 0.723 % ($p = 0.70$) (8 episodes in 3 hearts). When comparing the APD of the shock-induced beat with the subsequent sinus beat, variation was again small with a -0.57 ± 2.225 % ($p = 0.98$ compared with consecutive sinus beats) change. Additionally, there is minimal spatial variation across the heart, with no significant changes in action potential duration closer to the electrodes.

Diastolic intervals (DI) were also compared for stimulation strength nanosecond shocks and sinus beats. Here, there is an increase of the post shock DI compared to the pre-shock DI, 70.6 ± 5.275 %. However, this increase is temporary, with the second post-shock DI being 1.43 ± 3.96% of the pre-shock DI. Thus the change in diastolic interval is transient, though significant ($p < 0.0001$).

A similar comparison was performed on defibrillation-strength shocks in 5 hearts, looking at the post-shock DI compared with the second post-shock DI and the second compared with the third post-shock DI. See Figure 16. The diastolic interval immediately post-shock is 58.9 ± 8.95% longer than the following DI. This is significantly longer when compared with the second and third post-shock intervals, -1.514 ± 1.01% ($p = 0.0002$). This suggests that the effects of the shock on the diastolic interval are transient, and the heart returns to normal soon after the shock. It should be noted that a similar increase in diastolic interval also occurs after millisecond defibrillation-strength shocks [49].

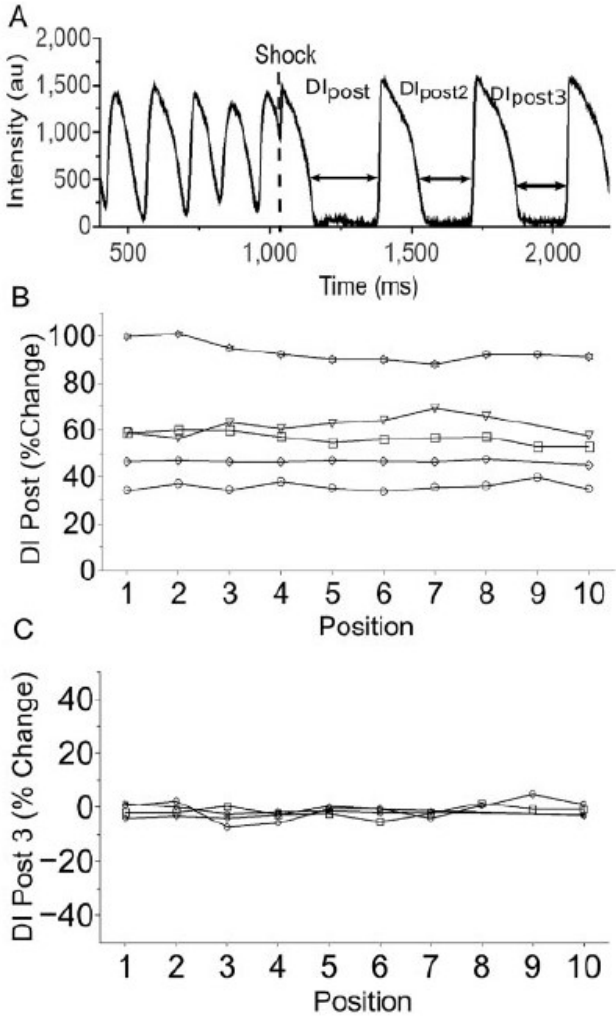

Figure 16. Effect of nanosecond defibrillation on diastolic interval in 5 hearts. A) Sample optical mapping recording from the epicardium showing ventricular tachycardia terminated by a defibrillation shock. B) Percent change of the first diastolic interval (DI_{post}) compared to the second diastolic interval (DI_{post2}) as a function of electrode position for 5 hearts. Position 1 is closest to the cathode and 10 is closest to the anode with all other positions spaced evenly between. Each different symbol represents a different heart. C) Change of DI_{post3} relative to DI_{post2} as a function of electrode position for 4 hearts.

3.3 Discussion

The effectiveness of 300 ns defibrillation was demonstrated, with reliable defibrillation achieved with energies that are almost an order of magnitude smaller that for 10 millisecond monophasic defibrillation. Additionally, a single defibrillation-strength shock caused no detectable uptake of propidium iodide, indicating a lack of electroporation and tissue death. No lasting electrophysiological changes were observed in the optical mapping traces. There was no baseline shift, which would have indicated electroporation, and there was no change in the action potential duration or shape. The diastolic interval immediately following shock application was significantly prolonged, however this reverted to normal after the subsequent action potential.

3.3.1 Mechanism of defibrillation

The external electric field applied to the heart during a defibrillation shock causes a local change in the electric field at the cell membrane. If this change is large enough to overcome reach the stimulation threshold, an action potential will occur. If enough cells are activated simultaneously, stimulation or defibrillation can occur. An electric field can act on the cell membrane in one of two ways: via the direct electric field or through membrane charging by movement of ions.

In a dielectric medium, dipoles align with an external applied field. The alignment occurs on the timescale of the dielectric relaxation time constant,

$$\tau = {\varepsilon_0 \varepsilon_R}/{\sigma} \qquad \text{Equation 6}$$

where ε_0 is vacuum permittivity ($8.854 \cdot 10^{12}$ F/m), ε_R is the relative permittivity of the medium and σ is the conductivity [29]. The membrane will see the full effect of the direct electric field

after the relaxation time for the aqueous solutions in which it is immersed: the cytoplasm, extracellular space, blood, or Tyrode's solution. A typical relative permittivity value for cytoplasm is 72.7 and conductivity is 1.7 S/m, giving a relaxation time of 378 ps, similar to the other aqueous solutions. Thus dielectric relaxation occurs long before the end of the nanosecond shock and the tissue is exposed to the highest possible electric field value.

Additionally, due to the heterogeneous nature of the cell-medium system, there is an amplification of the electric field due to the differing relative permittivities of the cell membrane and the cytoplasm. This amplification is proportional to the ratio of the permittivities, and is approximately 20 [50].

However, for a shock of 300 ns duration, the defibrillation threshold is approximately 1 kV/cm [48]. Thus, even with a gain factor of 20, the electric field at the membrane is only ~20 kV/cm, or ~10 mV across the membrane. This perturbation is likely not of high enough amplitude to trigger an action potential, particularly since the stimulus only lasts for 300 ns, whereas most ion channels take between 10 and 100 μs to open [51].

It is unlikely that dielectric charging plays any significant role in membrane effects since the fields expected are lower than those required for stimulation and occur on a very short timescale. However, there is evidence that points toward conductive charging as the membrane charging mechanism. This mechanism is well established for millisecond shocks, with studies showing that for 5-10 ms shocks, 1-2 V/cm is sufficient to excite cardiac tissue [52] and 5 V/cm is sufficient for defibrillation [53]. The charging time constant for electric fields of this amplitude is in the low millisecond range [54, 55], ensuring that the membrane sees the full effect of the shock.

Some experimental data seems to contradict conductive charging as the mechanism. For example, the defibrillation threshold electric field for 300 ns defibrillation is around 1 kV/cm, 60 times higher than that for 10 ms defibrillation. Assuming that the required pulse duration shortens proportionally to the membrane charging time, this amplitude should require a shock duration around 170 μs. However, the charging time constant decreases at higher amplitudes as shown in experiments by Efimov et al. where the time constant for millisecond shocks decreases from 5 to 2 ms at the anode as the shock amplitude increases from 100 to 220 V [55, 56]. Thus, if the charging time constant decreases to 10-100 μs, the change in membrane constant may account for the stimulation and defibrillation thresholds observed for 300 ns shocks.

Additionally, our optical mapping data show that nanosecond shocks uniformly activate the bulk of the myocardium. The strong virtual electrodes of both polarities for millisecond shocks in similar experimental setups are not observed [57].

3.3.2 Energy reduction when compared to conventional defibrillation

Compared with the monophasic shocks used for conventional defibrillation, 300 ns achieved a reduction of energy by almost an order of magnitude. This compares favorably to the 30-50% reduction in energy made possible by transition to biphasic shocks from monophasic shocks [17-19]. Our results for the energy of 10 ms defibrillation (530 ± 35 mJ) are consistent with that found by previous studies using smaller electrodes sutured to the ventricular walls of Langendorff-perfused rabbit hearts (270 mJ) [58].

3.3.3 Tissue damage

A variety of markers for tissue damage were assessed, including TTC staining, PI staining, baseline shift, and further optical mapping trace analysis. In all markers, no lasting damage was observed. The prolonged first diastolic interval after the shock was the only change in the electrophysiological behavior. This result is consistent with the "stunning" seen in cardiac tissue after millisecond shocks [49] and does not suggest permanent tissue damage.

Electroporation, though not detected in our histological or optical mapping analysis, is known to play an important role in defibrillation and a reduction of vulnerability to proarrythmic effects [16]. It is possible that some PI uptake occurred during nanosecond defibrillation shocks, but the fluorescence was below the detection limit of the microscope. Nanosecond pulsed electric fields are known to have different effects on the permeability of the cell membrane when compared to longer shocks [59-61]. It is possible that nanosecond shocks electroporate or electropermeabilize cells at lower energies, resulting in higher leak currents and the depolarization of the cell. This topic will be discussed in further detail in Chapter 5.

3.4 Conclusion

The efficacy of 300 ns shocks for defibrillation and stimulation was evaluated. In comparison with 10 ms shocks, nanosecond shocks require almost an order of magnitude less energy to defibrillate. No tissue damage was observed in histological analysis. No lasting electrophysiological changes were observed from optical mapping traces. This work was published in *Cardiovascular Research* [48].

CHAPTER 4:

SAFETY FACTOR OF NANOSECOND DEFIBRILLATION

4.1 Introduction

In the results presented in Chapter 3, we showed that single defibrillation-strength shocks cause neither propidium iodide uptake nor tissue death (as determined with a tetrazolium chloride stain), and that the only immediate electrophysiological effect is a prolongation of the diastolic interval directly following the shock.

Further studies in cardiomyocytes measured PI uptake at five times the stimulation threshold for various pulse durations, with 200 ns shocks resulting in 1.7 times less uptake than 800 ns shocks and 4 times less than 10 μs shocks [25]. To determine whether shorter pulses also create less damage in myocardial tissue, we investigated how the field strength of the electroporation ED50, as indicated by propidium iodide uptake, compares to the defibrillation ED50 field strength.

A complication in the design of this study was that while electric shock delivery with parallel plate electrodes may be the best approximation of clinical defibrillation, this geometry exposes the whole heart to the applied electric field and would allow for only one shock application per heart, resulting in an excessive use of rabbits. To avoid this limitation, we inserted a pair of needle electrodes into the myocardium in order to apply fields in a localized manner; as a result, we were able to place about 10 applications per heart. To find the relationship between the shock-induced fields in the needle electrode and parallel plate electrode geometries, we used electrostatic modeling of both geometries as detailed in Chapter 2.

To achieve the best estimation of the electroporation ED50, we applied voltages of amplitudes that resulted in different degrees of staining. Since the electric field drops off with distance from the electrodes, higher applied voltages will result in a larger radius of staining, and the effect of different voltages can be combined to determine ED50 with greater accuracy. Initial modeling and experimental results show that applying the ED50 defibrillation voltage for the parallel plate electrodes (DV) to the needle electrodes results in a staining radius of slightly less than 1mm (for both 10 ms and 300 ns shocks); since the needle electrodes are separated by 4 mm, the stained regions around the two electrodes are clearly separated in this scenario. An applied voltage of twice the parallel plate ED50 defibrillation voltage (2 DV) results in a staining radius of approximately 1 mm. For an applied voltage of 5 DV, the staining radius typically exceeds 2 mm and the stained regions around the electrodes begin to overlap. These degrees of staining for 1 DV, 2 DV, and 5 DV were conducive to an accurate determination of ED50, so we used these shock amplitude in our staining experiments. The defibrillation thresholds determined previously for the parallel plate geometry are 37 V for 10 ms shocks and 2.35 kV for 300 ns shocks across an electrode spacing of 3 cm [48], so the voltages applied to the needle electrodes were 37 V, 74 V, and 185 V for 10 ms and 2.35 kV, 4.7 kV, and 11.75 kV for 300 ns. All experiments had a 47 Ω resistor placed in series for impedance matching between the load and the pulsers. There was some variability in applied voltages (typically ~5-10%) due to the limited accuracy in the control of the charging voltage. To account for this variability, the applied voltage is experimentally measured for each shock and the results are used in our model calculations.

4.2 Staining Analysis

From the electric field distribution that we calculated for the needle electrode geometry, we extracted electric field values on the plane that intersects the electrode axes and the surface of the

cardiac shell in proximity to the electrodes. These values were then used to determine the electric field values at each pixel location of the experimental fluorescence images. To illustrate the shape of the electric field, we also extracted several isolines (i.e. lines of a constant value of the electric field).

After equilibration in the Langendorff-perfusion setup, the electrode needles were inserted perpendicular to the myocardial surface at 10 to 16 locations, and a single shock was applied at each location. In total, the treatment duration was between 10 and 15 minutes. For the 9 experiments performed, the 10 ms and 300 ns treatments were performed in alternating starting order, with randomized application of the three shock strengths within each set of shock durations. Additionally, one to two sham exposures were performed in each heart, where the electrodes were inserted into the myocardium but no shock was applied.

To quantify the electroporation ED50 electric field for the surface images, we used the needle electrode field distribution and bilinearly interpolated to calculate the electric field at each pixel location (using ImageJ). Pixels with at least twice the background fluorescence level were considered above damage threshold. We then determined the fraction of pixels above the damage threshold as a function of electric field strengths (using increments of 5 V/cm for the 10 ms shocks and 120 V/cm for the ns shocks). The electroporation ED50 was then taken to be the electric field value where 50% of the pixels were stained.

For the cross-sectional images, the cutting plane often differed slightly from the plane of electrode insertion. Thus, the fluorescence intensity along the electrode axis was evaluated to determine the tissue depth at which the fluorescence intensity was the strongest. At this depth, the fluorescence signal was quantified along a line (7 pixels wide), perpendicular to the

electrode. The electroporation ED50 was then determined as for the surface staining images in the rectangular area 7 pixels tall and 200 pixels wide, approximately 0.14 by 4 mm. In this case, since fewer pixels were used, the electric field increments were increased to 10 V/cm for the 10 ms shocks and 200 V/cm for the ns shocks.

Once the safety factor was determined for each cross-section or surface staining image, the results for each 300 ns and 10 ms were averaged and the standard deviation and standard error of the mean (SEM) were calculated. Group results are presented as mean ± SEM. These results were compared using two-tailed, unpaired Student's t-tests where $p<0.05$ was considered statistically significant.

4.2.1 Surface Staining

As shown in Figure 17A, there is an increase in stained area as the applied voltage increases for both ms and ns shocks. The isolines depicted show 15 $E_{max,DV}$, 6 $E_{max,DV}$, and 3 $E_{max,DV}$ from inside to outside. It can be seen that for all durations that the 6 $E_{max,DV}$ isoline approximately corresponds to the area of staining. However, there is some anisotropy observed, particularly at the highest voltage application for each shock duration. This holds true for most of the analyzed images and is likely caused by the anisotropic structure of cardiac tissue.

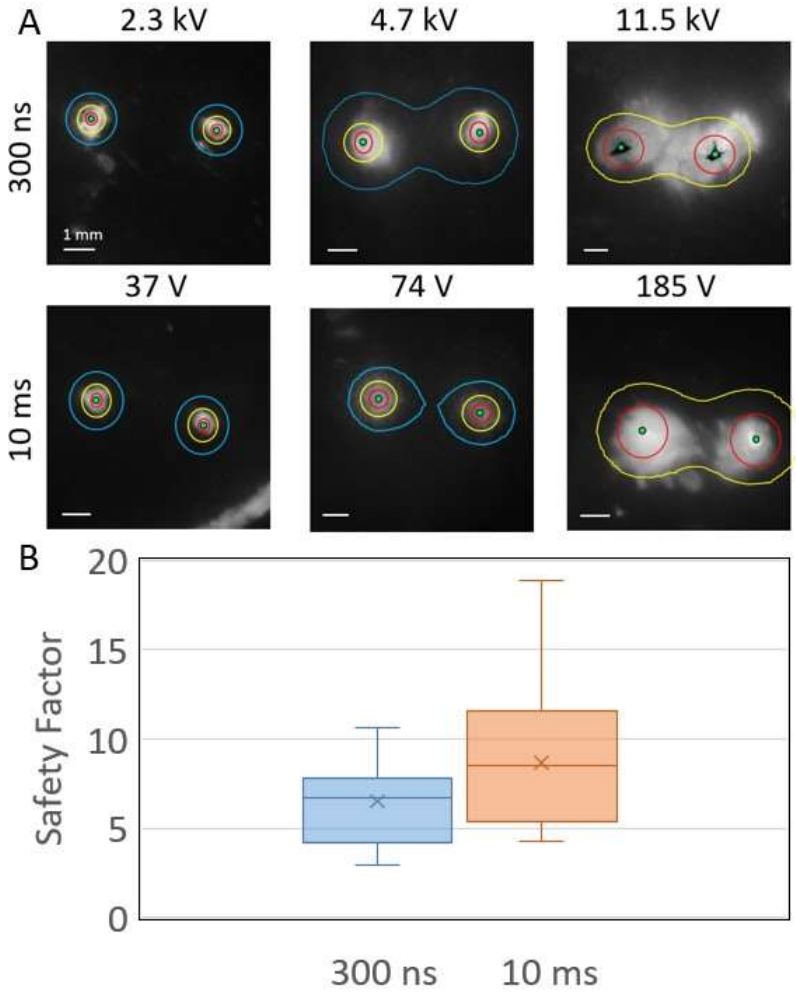

Figure 17. PI staining for 300 ns and 10 ms shocks of different field strength. A) Representative PI staining examples for both 300 ns and 10 ms with applied voltages corresponding to 1, 2, and 5 defibrillation thresholds at 1 mm from the electrodes. The isolines show where the field strength equals to 15 $E_{max,DV}$ (red), 6 $E_{max,DV}$ (yellow), and 3 $E_{max,DV}$ (blue). In the case of the strongest applied voltage, the 3 $E_{max,DV}$ isoline is omitted because it runs mostly outside the field of view. B) The box plot above shows the safety for the surface staining results for 300 ns (n=26) and 10 ms shocks (n=23). The averages are denoted with an x, the box shows the first quartile to the third quartile with the median intersecting the box, and the whiskers denote the maximum and minimum.

Evaluation of 26 applications of 300 ns shocks and 23 applications of 10 ms shocks resulted in an average safety factor of 6.50±0.51 for 300 ns shocks and 8.69±0.80 for 10 ms shocks. This difference is statistically significant ($p=0.02$).

4.2.2 Cross-sectional Staining

Additionally, in 7 out of 9 experiments, cross-sections of the tissue in the electrode plane were imaged (see Figure 5). Quantitative analysis was performed as for surface staining. In this case, the safety factor is 5.38±0.52 for 300 ns shocks and 6.29±0.51 for 10 ms shocks, and the difference is not significant ($p=0.22$).

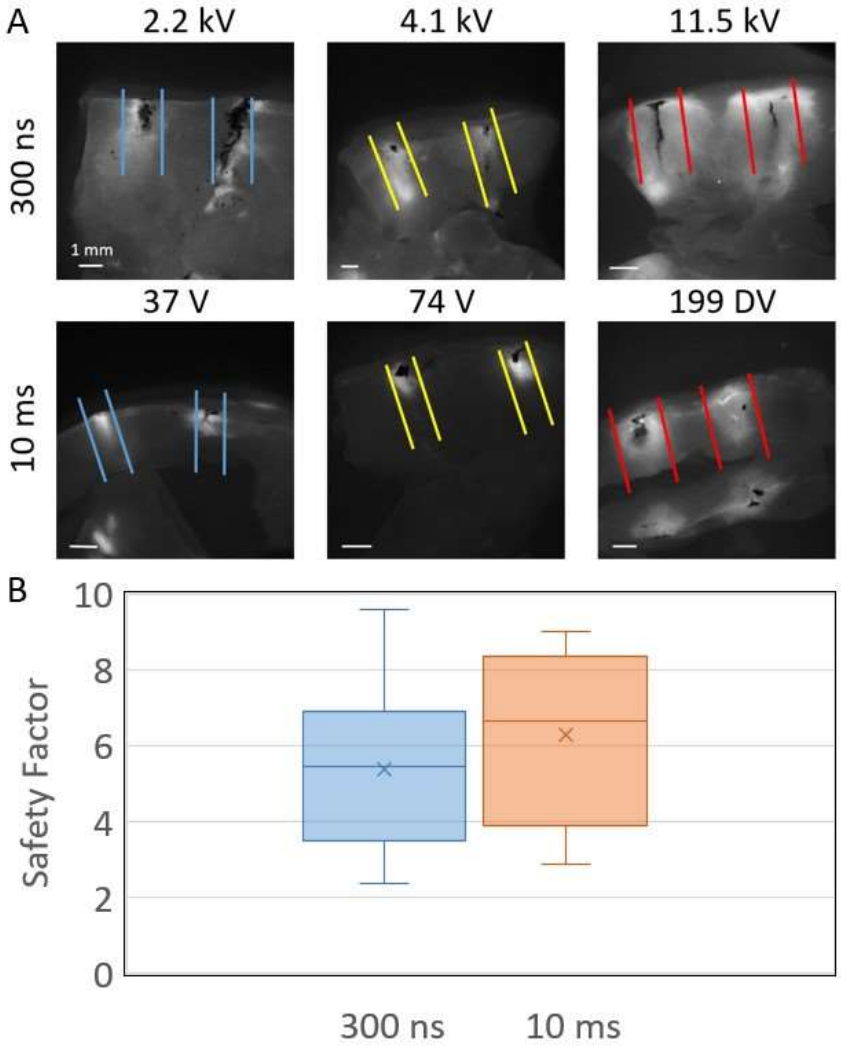

Figure 18. PI staining for shocks of different field strength. A) Representative examples for PI staining of tissue sections in the needle plane, for both 300 ns (top) and 10 ms (bottom). The parallel lines denote the isolines for 3 (blue), 6 (yellow), and 15 (red) $E_{max,DV}$. B) The box plot shows the safety factor for the cross sections for 300 ns (n=18) and 10 ms shocks (n=17). The averages are denoted with an x, the box shows the first quartile to the third quartile with the median intersecting the box, and the whiskers denote the maximum and minimum.

4.3 Discussion

We have shown that the safety factors of 300 ns pulses and 10 ms defibrillation are comparable. In isolated rabbit hearts, shocks were delivered with a pair of penetrating electrodes, and there a slight difference in electroporation as determined by propidium uptake. The numerical values of the safety factors as determined by surface staining are about 6.5 for nanosecond and about 8.7 for millisecond defibrillation; their determination relied on computer simulations that related the electric field distributions for parallel plate electrode stimulation and penetrating electrode stimulation.

4.3.1 Surface versus and cross-section analysis

Our analysis of surface staining yields a safety factor of 6.50 for 300 nanosecond shocks and 8.69 for 10 ms shocks ($p=0.02$); the analysis of cross sections gave a safety factor of 5.38 for 300 ns shocks and 6.29 for 10 ms shocks ($p=0.22$). Both analyses have their advantages and drawbacks. For surface analysis, fluorescence at the site of interest can easily be detected, but the surface is slightly deformed by the insertion of electrodes, which distorts the electric field. Deformation is not a concern for the cross-section analysis, but there, it is harder to ensure that fluorescence is measured precisely in the electrode plane. Overall, we observed greater consistency in the cross-section analysis and have greater confidence in its results. Combining the results of both analysis, we conclude that the safety factor is in the range from five to nine, and that we observe a slightly higher safety factor for millisecond shocks than for nanosecond shock, although it is not clear whether this difference is statistically significant.

4.3.2 Implications for nanosecond defibrillation

Our experiments were conducted with a penetrating electrode configuration to allow for multiple shock applications per heart, and we used computer modeling to select shock amplitudes from a parallel electrode configuration that is more representative of how electric fields are applied during defibrillation. The proper interpretation of our results requires some discussion of the modeling approach. In our simulations of the parallel plate geometry, we observed the strongest field at those parts of the endocardium that are facing the electrodes (see Figure 11). It needs to be kept in mind that the propidium-stained areas that we determine in Figure 17 do not directly quantify the damage to be expected with defibrillation in the parallel-plate configuration. While the fact that significant propidium uptake starts at fields around 6 $E_{max,DV}$ indicates that we should expect to see damage at 6 DV for parallel plate electrodes, the extent of the expected damage also needs to consider the field distribution in the parallel plate configuration as shown in Figure 11. If we apply, for example, 7 DV, Figure 11 shows that in the walls facing the electrodes, the inner parts, up to about the center of the wall, will be exposed to more than 6 $E_{max,DV}$. We would therefore expect that this portion of the walls may be damaged and would take up propidium if we performed an experiment in this electrode configuration. The cardiac geometry used is of course an approximation, but a similar interpretation is necessary in more detailed reconstructions of cardiac anatomy. Note that these considerations do not affect our conclusion that the safety factors of millisecond and nanosecond defibrillation are similar, which was based purely on the penetrating electrode data.

Similar safety factors of nanosecond and millisecond defibrillation may actually translate into nanosecond defibrillation being preferable if field uniformity is also considered. Several studies have suggested that the fields induced by nanosecond shock are more uniform that those of

millisecond shocks [30, 62]. The field strength of a defibrillation shock needs to be chosen such that it excites the bulk of the tissue; for a more uniform field this should mean that less tissue is exposed to fields exceeding the damage threshold.

4.3.3 Comparison to earlier results on electroporation with millisecond pulses

While the results reported here are the first assessment of electroporation of cardiac tissue with nanosecond pulses, electroporation after millisecond shocks has previously been studied.

Wang et al. showed that for an internal coil-shaped electrode with a reference electrode not touching the heart, PI staining after defibrillation is only observed close to the internal active electrode [63]. In this case, the highest electric field would have been next to the active electrode and decreasing with distance. This is a different geometry than our needle electrode configuration, but is consistent with our findings that electroporation is only seen close to the needle electrodes where electric field is higher than at greater distances.

Additionally, Al-Khadra et al. determined the defibrillation and electroporation thresholds for a coil electrode placed in the ventricular cavity with the second electrode 2 cm away [16]. The shock waveform was a monophasic 8 ms truncated exponential. They found a safety factor of about 1.3, substantially below what we report here, but this should be expected since the coil electrodes used by Al-Khadra generate a much more heterogeneous electric field. Since defibrillation requires a certain minimum field almost everywhere in the heart, including in areas where the heterogenous field is low, the areas where the heterogeneous field is high will experience a much higher field and therefore be more likely to exhibit electroporation.

The similar safety factors of nanosecond and millisecond shocks are unexpected, however, in light of recent experiments that exposed single cells to shocks of 200 ns to 2 ms duration [25]. In these cells, it has been shown that for shocks at five times the stimulation threshold, cells take up the least amount of PI for a 200 ns shock duration when compared to 800 ns, 50 μs, and 2 ms. However, even for 200 ns shocks, there was still significant PI uptake, and repeat excitation of cardiomyocytes at the stimulation threshold using nanosecond shocks is not possible without electroporative damage. It should be noted that in whole hearts, the defibrillation threshold is almost six times higher than the stimulation threshold for 300 ns [48, 64] Thus, for whole heart experiments, there must be other factors at play that cause the safety factors of 300 ns and 10 ms to be similar and much greater than one.

4.4 Conclusion

We tested the safety factors of nanosecond defibrillation in comparison to millisecond defibrillation and found little difference. Surface staining results show a safety factor of 6.50 for 300 nanosecond shocks and 8.69 for 10 ms shocks, $p=0.02$. Cross-sectional results show a safety factor of 5.38 for 300 ns shocks and 6.29 for 10 ms shocks, $p=0.22$. When combined with our previous result that nanosecond shocks can defibrillate at lower energies, nanosecond defibrillation becomes a more viable option for low-energy defibrillation.

CHAPTER 5:

STIMULATION STRENGTH-DURATION CURVE

5.1 Introduction

To obtain data over a broader range of pulse durations, the strength-duration curve for stimulation was obtained from 200 ns to 10 ms. Since stimulation requires lower energy than defibrillation, and does not require the induction of fibrillation beforehand, a larger number of data points can be collected in each heart before it deteriorates. The strength-duration curve can help determine the susceptibility of tissue to shocks of varying duration, particularly when compared to membrane charging models. Additionally, the curve can help predict the defibrillation threshold for shock durations that have not yet been studied.

For these experiments, for each recording, 5, 10 ms shocks were applied to the heart via plate electrodes at a frequency slightly faster than sinus rhythm (3-5 Hz). The subsequent shock was a nanosecond shock, after which pacing with 10 ms shock resumed until the end of the recording (3-5 seconds total). The amplitude of the nanosecond shock was slowly increased until the stimulation threshold was reached, and the pulse duration was selected randomly. Each point is the average of between one and four stimulation results with the electric field calculated by dividing the applied voltage by the electrode spacing. 6 hearts were used for these experiments.

5.2 Results

The stimulation strength-duration curve from 10 ms to 200 ns is shown in Figure 19A. As expected, the required electric field for stimulation increases with a decrease in pulse duration.

At pulse durations longer than 1 ms, the curve flattens to rheobase, the minimum electric field required for stimulation of theoretically infinite duration. At durations shorter than the time constant (~200 μs), the curve transitions to a negative slope. Since membrane charging is not complete by the time the shock is over, the membrane sees a fraction of the applied electric field, and a higher applied electric field is required to stimulate the tissue.

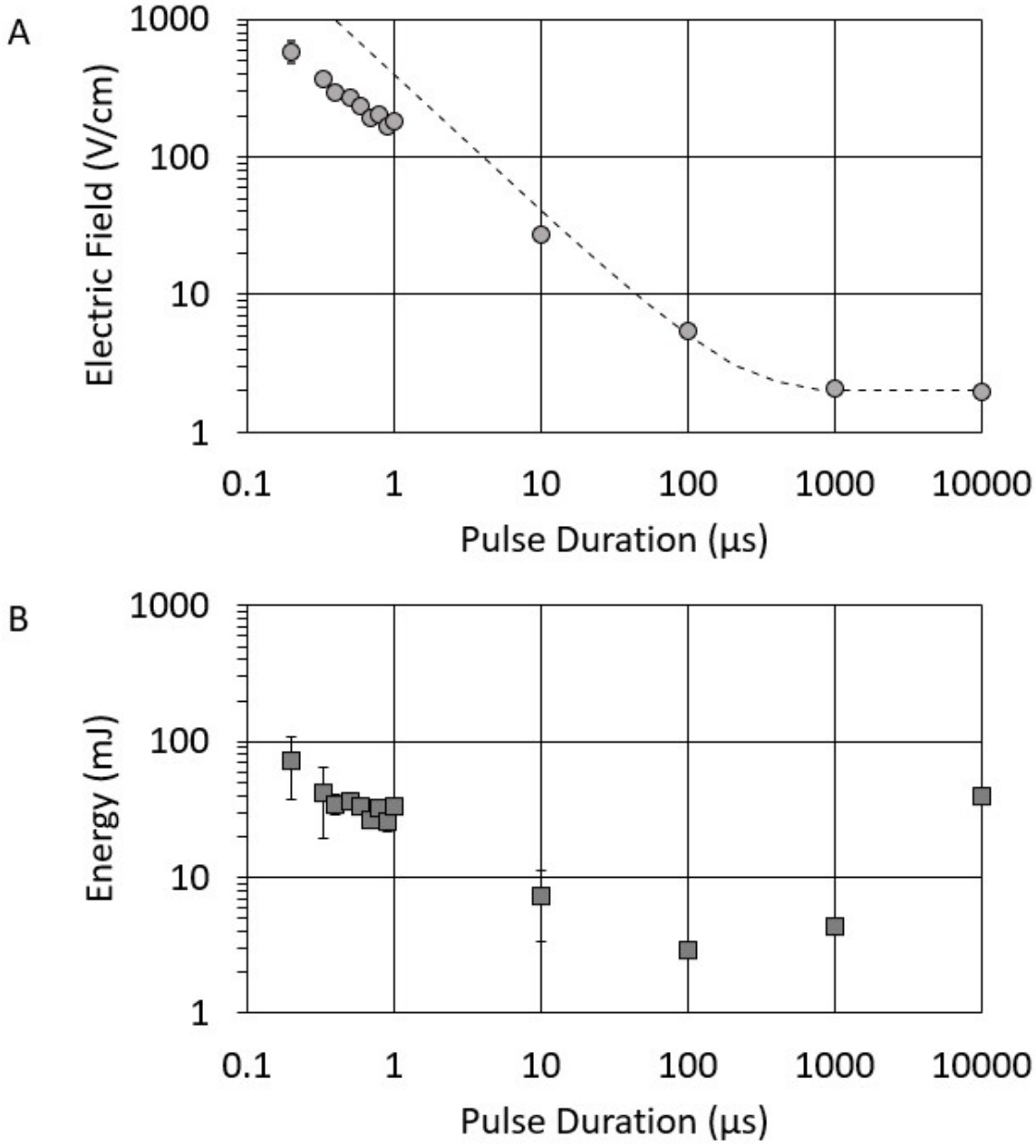

Figure 19. Strength-duration curve for stimulation in Langendorff-perfused rabbit hearts with aluminum plate electrodes. The electric field (A) is found by dividing the applied voltage by the distance between the electrodes. The dashed line shows the theoretically predicted required electric field across the electrodes if membrane charging is governed by the equation $E_{th} = \frac{b}{\left(1-e^{-d/\tau}\right)}$*. The energy (B) is found by integrating the product of the current and voltage waveforms.*

When the deposited energy is calculated at the stimulation threshold for each shock duration by integrating the multiple of the voltage and current waveforms (Figure 19B), the minimum is for 100 μs, and shocks in the 100s of nanoseconds and 10s of milliseconds are on the same order of magnitude [64]. This differs from the results of the defibrillation experiments where 300 ns shocks required almost an order of magnitude less energy to defibrillate compared to 10 ms shocks. However, knowing that the safety factors of both pulse durations are very similar, and most attempts at repeated stimulation in cardiomyocytes result in injury [25], it is possible that the stimulation and defibrillation thresholds in whole hearts are closer together for shorter shocks than longer shocks.

In all hearts in which nanosecond stimulation was attempted ($n=6$) and over the range of durations from 200 ns to 1,000 ns which was studied here, we were always able to stimulate cardiac tissue with sufficiently strong nanosecond stimuli, unless the heart had been damaged by repeated stimulation (see below). In total, 29 stimulation thresholds were determined successfully.

5.2.1 Optical mapping trace analysis

In 8 hearts, we stimulated periodically with millisecond stimuli and replaced a single millisecond stimulus with a nanosecond stimulus. Then we compared the APD induced by the millisecond pulse immediately before the nanosecond pulse to the APD induced by the nanosecond pulse. We found that the APD is indistinguishable from that of millisecond stimulation (6.26 ± 9.45%).

For the same stimulation sequence as above (periodic millisecond stimulation, with a single stimulus replaced by a nanosecond stimulus), we also compared the APD of the millisecond

stimulation immediately preceding the nanosecond stimulus to the APD of the millisecond stimulation immediately following the nanosecond stimulus. This allows us to assess whether the nanosecond stimulation has short-term effects that affect the normal excitation physiology.

We found that in 8 hearts, the APD before and after the nanosecond stimulus is indistinguishable (-0.02 ± 3.81%)

To assess the potential damage of multiple nanosecond shocks to cardiac tissue, we compared action potential durations in response to a millisecond pacing shock before and after 20 nanosecond shock applications. Each of these shock applications includes between 5 and 10 millisecond shocks.

The change in the APD from the beginning of the experiment to the point at which 20 ns shocks had been applied is not statistically significant (4.72 ± 8.06%).

Additionally, traces were analyzed for any changes in baseline, which would indicate electroporation and deterioration of cell's ability to maintain equilibrium membrane potential, and none was observed.

5.2.2 Repeat stimulation without damage

Additionally, experiments were performed with trains of five nanosecond pulses of varying duration (200-1000 ns) at 4-5 Hz, and the heart was not paced otherwise. Shock amplitudes are typically within 50% of stimulation threshold, above or below. We were able to apply hundreds of nanosecond shocks to the heart without signs of electrophysiological damage. For these experiments, the average number of ns pulses applied was 215 ± 30. The experiment was ended

when the internal pressure at the aortic cannula exceeded 120 mmHg even with the flow rate reduced to 10-15 mL/min, the heart no longer sustained a sinus rhythm, or the optical mapping signal amplitude decreased below noise levels.

5.3 Discussion

In summary, the stimulation strength-duration curve for whole hearts was determined down to 200 ns. There was no sign of electrophysiological damage in the optical mapping traces, and we were able to repeatedly stimulate with nanosecond shocks.

It should be noted that the stimulation thresholds presented here (200 V/cm for 1000 ns) are low compared to results published in isolated cardiomyocytes where the stimulation threshold for 1000 ns shocks is on the order of 1 kV/cm [25]. However, it should be kept in mind that stimulation in whole heart preparations requires the excitation of only a small patch of tissue. Model results from the safety factor simulations seen in Figure 11 show an enhancement of the electric field at the inner surface of the myocardium. The simplicity of this model possibly even underestimates the maximum electric field as it does not account for tissue inhomogeneities that could further enhance the electric field. Thus, the electric field values presented here as voltage divided by electrode spacing are likely lower than the electric field seen at the point of stimulation.

However, the 2.35 kV defibrillation threshold for determined previously for 300 ns shocks would have an electric field of approximately 800 V/cm with the voltage over distance calculation, which is consistent with the stimulation results seen here.

5.3.1 Comparison with Blair Model

Strength-duration curves for excitation in neurons follow the relationship predicted by the Blair fit described in Equation 7, with *d* being the pulse duration and *E* being the electric field across the membrane required for stimulation.

$$E = \frac{b}{\left(1-e^{-d/\tau}\right)} \qquad \text{Equation 7}$$

The rheobase electric field, *b,* is the minimum field required for a shock of theoretically infinite duration. The membrane time constant, τ, is the point at which the slope of the curve transitions to its final value.

The dotted line in Figure 19 shows the predicted curve based on equation 7 with a charging time constant of 200 μs (the best fit for pulse durations (*d*) longer than 10 μs) and rheobase of 2 V/cm. It can be seen that for shorter pulse durations, the prediction fails, and the electric field required for stimulation is proportional to $d^{-0.75}$.

This is contrary to the results of the experiments Rogers et al. performed on frog gastrocnemius preparations (including a portion of the sciatic nerve) to determine the strength-duration curve down to 1 ns [26]. The experimental results match closely with the Blair model calculated with a time constant of 270 μs and a rheobase voltage of 313 mV. The only discrepancy is the 1 ns datapoint. However, the shock waveform for 1 ns has a total pulse duration closer to 8 ns, which would place this data point on the curve. The experimentally determined time constant is 285 μs, indicating that the electrical shocks are stimulating nerves (τ≈0.2 ms), not directly the muscle (τ≈2.0 ms). Other experiments performed in isolated frog nerves also find that the excitation threshold for 12 ns shocks is on the same order of magnitude as the gastrocnemius results [27].

This corroborates the conclusions of Rogers et al. that they were stimulating the sciatic nerve to trigger muscle contraction. Excitation with nsPEF in neurons follows the strength-duration curve predicted by conductive charging.

However, in cardiomyocytes of several different species, the discrepancy between the expected strength-duration curve based off Equation 7 and experimental results is even greater [25]. In this case, the electric field at the stimulation threshold is approximately proportional to $d^{-0.5}$ at shorter pulse durations. So the Blair model is not sufficient to explain the electric field effects at the amplitudes required for nanosecond stimulation in cardiac tissue.

5.3.2 Mechanism of cardiac tissue stimulation

The conductive charging mechanism seems sufficient to explain nanosecond stimulation results of neurons as seen by the good fit using the Blair model. However, in stimulation experiments performed on cardiac cells and tissues, there is a deviation from the expected electric field for pulses of varying duration. In the nanosecond regime, a lower electric field than expected is needed to compensate for the shorter pulse duration. Figure 19 shows the strength-duration curve for stimulation in a Langendorff-perfused rabbit heart using parallel plate electrodes. The dotted line shows the predicted curve based on Equation 6 with a charging time constant of 200 μs (the best fit for pulse durations (d) longer than 10 μs). The Blair model predicts a slope of -1 at durations shorter than 100 μs. However, the results show that the electric field required for stimulation is proportional to $d^{-0.75}$ at those pulse durations. This indicates that capacitive membrane charging cannot be the sole mechanism of nanosecond defibrillation and stimulation

One way of describing the results in the previous section is that the charging time "constants" in cardiac cells and tissues becomes shorter for higher electric fields. The effects of increasing pulse amplitude on membrane charging were also discussed in Section 3.3.1 [55]. In Langendorff-perfused rabbit hearts, high amplitude shocks were applied during the action potential plateau. The deflection in the optical mapping trace was analyzed to give the charging time constant. It was discovered that regardless of where during the action potential the shock was placed, the charging time constant decreased for higher applied voltages. The results were repeated with lidocaine to block the sodium channels. However this did not affect the trend of faster time constants for higher fields.

If this trend is maintained for pulses of much higher amplitude, this could explain discrepancy in expected E-field amplitude required for stimulation of cardiac cells and tissues for pulses of shorter duration. At 200 ns, keeping all else constant, a charging time constant of ~50 μs instead of 200 μs would account for the discrepancy shown in Figure 19.

5.3.3 Electropermeabilization before stimulation

One possible explanation for the greater effectiveness of nanosecond shocks to stimulate tissue is that electropermeabilization occurs before stimulation. As cells are electropermeabilized, ions are allowed to flow down their concentration gradient, and sodium and calcium enter the cell. This depolarizes the cell even if the change in the transmembrane voltage due to the applied electric field is not large enough to reach the stimulation threshold voltage. If this depolarization is large enough, an action potential will occur. This effect has been seen in chromaffin cells where, following application of a 12 ns shock, cells are depolarized by sodium entry. Sodium

bypasses sodium channels, entering the cell through nanopores or non-specific cation channels [39].

It has been shown that for isolated cardiomyocytes, it is possible to stimulate with nanosecond pulsed electric fields; however, the electroporation threshold is typically below the stimulation threshold and after repeat stimulation, the cell stops responding [25, 65]. Thus, for these experiments in cardiomyocytes, electroporation occurs before stimulation. This would allow for the influx of calcium ions and calcium induced calcium release. In the study by Azarov et al., it was shown that action potential generation by 200 ns shocks is dependent on extracellular calcium. Calcium transients did not occur in the absence of extracellular calcium, demonstrating that electroporation of the endoplasmic reticulum is not the primary cause of stimulation. Additionally, calcium transients still occurred in the presence of verapamil and tetrodotoxin, ruling out ion channel involvement. These results seem to indicate that electroporation, allowing calcium to enter the cell and triggering calcium induced calcium release from the endoplasmic reticulum is the primary mechanism for action potential generation of nanosecond shocks in cardiomyocytes.

However, in experiments showing nerve excitation at 12 ns, no indicators of electroporation were observed after 1 minute of tetanus at or above the stimulation threshold [27]. Rogers et al. also observed no evidence of electroporation in their study, which stimulated the sciatic nerve. One possible explanation is a difference in charging time constants for the different cell types or tissues [66]. Ion channel response to a change in membrane potential takes at least 11 μs [41]. Thus, the membrane must stay above the stimulation threshold for that duration. A nanosecond shock must have a high amplitude to achieve this condition, while remaining below the

electroporation threshold. In a cell with a long time constant, the membrane discharge time is longer, allowing for a lower charging voltage and staying below the electroporation threshold. It is expected that the arrangement of cardiomyocytes into cardiac tissue increases the time constant due to gap junctions and lower extracellular conductivity. This would explain why we see a shallower slope for the cardiomyocyte strength-duration curve than that for whole hearts in the nanosecond regime.

One set of evidence against electroporation as the mechanism for stimulation is that no propidium iodide uptake was observed for defibrillation-strength nanosecond shocks in Langendorff-perfused hearts [48]. However, it is possible that propidium iodide (PI) fluorescence in this study was present but below the detection limit, as fluorescence increases nonlinearly at conditions close the permeabilization threshold. PI also has a lower fluorescence response at low concentrations compared to YO-PRO-1, for example [67]. Additionally, no baseline shift was observed during stimulation and defibrillation experiments. It is possible that minimal or reversible electroporation occurs, with no effect on electrophysiology, and that pores are resealed during the time between shocks.

5.4 Conclusion

The stimulation strength-duration curve for Langendorff-perfused rabbit hearts was determined for shocks of duration 200 ns to 10 ms. There is no change in action potential duration when comparing any nanosecond shocks with millisecond shocks. Additionally, even after hundreds of nanosecond shocks, the heart still responded normally to stimuli and did not exhibit any changes in action potential duration or baseline shift. The curve deviates from the values predicted by

capacitive membrane charging below 10 μs, possibly indicating electroporation or some other mechanism by which nanosecond shocks charge membranes more efficiently.

CHAPTER 6:

MHZ DEFIBRILLATION

6.1 Introduction

Despite the low energy properties and safety of nanosecond defibrillation, there are hurdles to its implementation in clinics and hospitals. The pulsers required to produce such short shocks are typically large and made of many feet of coaxial cables or large capacitor banks. This puts a limitation on portability. Additionally, the high voltages required for nanosecond defibrillation require large power supplies and pose a safety hazard.

It may be possible to overcome these limitations with a recently developed technique called megahertz compression. Pakhomov et al. showed that it is possible to excite and electroporate cells using a pulse train of nanosecond shocks of much lower amplitudes at MHz frequencies [38]. For trains of 5 and 100 shocks of 340 ns duration, the amplitude required for nerve stimulation decreases at pulse repetition frequencies above approximately 5 kHz. For 100, 200, and 400 ns shocks, the stimulation amplitude depends only on the time-averaged amplitude and burst duration. For a burst of 100 shocks of 200 ns duration at 3.3 MHz, the time-averaged stimulation threshold is the same as the threshold for a 300 μs shock that is the same duration as the pulse train.

In cardiomyocytes, MHz compression is also effective in reducing the stimulation electric field threshold [38]. If the energy reduction seen for 300 ns shocks compared with 10 ms shocks (Section 3.2.2) also occurs for the lower amplitude nanosecond shocks used during MHz compression compared with a single long shock, this could provide a work-around for the

requirement of bulky, high voltage pulsers and improve the feasibility of nanosecond defibrillation.

To determine whether MHz compression results in defibrillation at lower energy or average voltage than defibrillation with a long shock of the same duration as the pulse train as well as the clinical standard for defibrillation, we compared trains of 1,000 pulses of 1000 ns duration at 0.4 MHz with single pulses of 2.5 ms duration and 5+5 ms biphasic shocks. See Figure 20 for a representative trace of a section of the MHz pulse train.

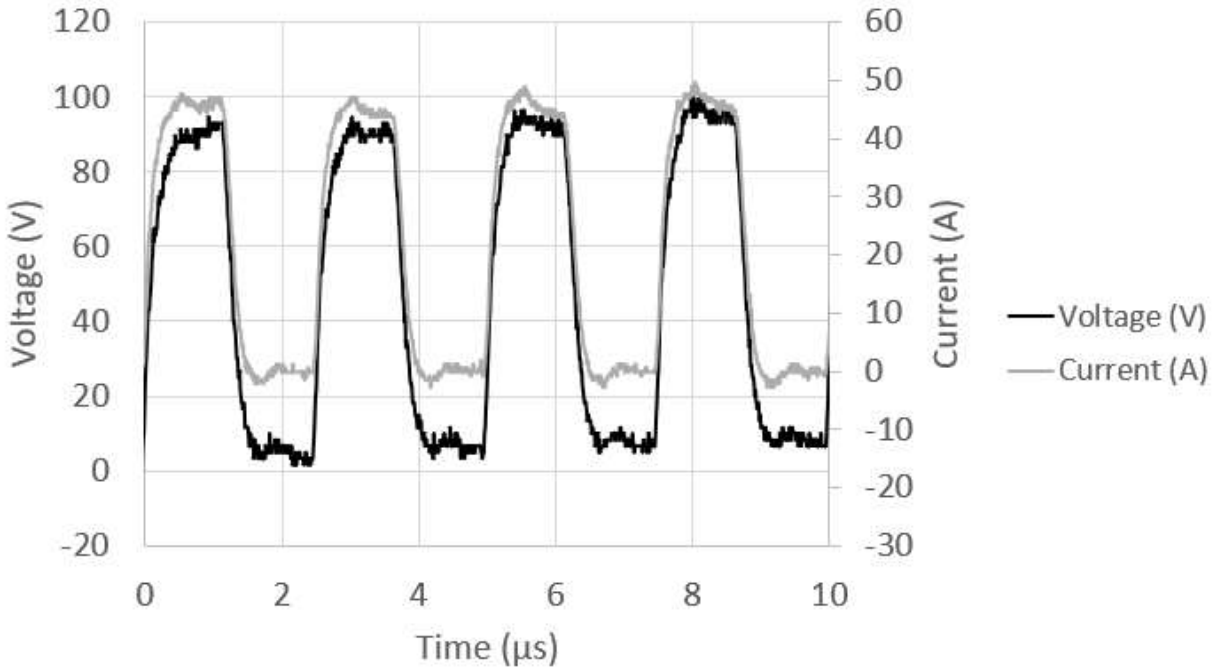

Figure 20. Voltage and current waveforms for the first 10 us of the MHz pulse train.

6.2 Results

6.2.1 Defibrillation threshold electric field and energy

In 7 hearts, we determined the minimum voltage required for defibrillation. The defibrillation threshold electric field was calculated by taking the applied voltage and dividing by the electrode spacing at the center of the electrodes.

The results are summarized in Table 1. The average threshold electric field for defibrillation with MHz shocks is 40.9 ± 4.3 V/cm. This value is much lower than the stimulation threshold for a single 1000 ns shock (182.7 ±5.2 V/cm) as determined in Chapter 5. As expected, MHz compression reduces the electric field required for defibrillation.

Table 1. Experimental results for MHz compression experiments.

Pulse condition	Heart #	Threshold Field (V/cm)	Average Field Threshold (V/cm)	Difference in Average Field Threshold, MHz vs. ms (%)	Energy (mJ)	Difference in Energy MHz vs. ms (%)
1000, 1000 ns @ 0.4 MHz	1	46±2	21±1	-8.7	1106	17.2
2.5 ms	1	23±1	23±1	-	944	-
1000, 1000 ns @ 0.4 MHz	2	27±1	14±1	-6.7	371	86.4
2.5 ms	2	15±1	15±1	-	199	-
1000, 1000 ns @ 0.4 MHz	3	41±2	20±1	-16.7	692	20.3
2.5 ms	3	24±4	24±4	-	575	-
1000, 1000 ns @ 0.4 MHz	4	60±2	25 ± 1	4.2	1150	121.6
2.5 ms	4	24±3	24±3	-	519	-
5+5 ms	4	10+10 ±1	-	-	299	-
1000, 1000 ns @ 0.4 MHz	5	32±2	15±1	-21.1	-	-
2.5 ms	5	19±3	19±3	-	-	-
5+5 ms	5	9+9 ±1	-	-	-	-
1000, 1000 ns @ 0.4 MHz	6	48 ± 1	23 ± 1	-8.0	-	-
2.5 ms	6	25 ± 1	25 ± 1		-	-
5+5 ms	6	10+10 ± 1	-		-	-
1000, 1000 ns @ 0.4 MHz	7	32 ± 2	16 ± 1	-38.5	460	-31.0
2.5 ms	7	26 ± 2	26 ± 2		667	-
1.25+1.25 ms	7	12+12 ± 1	-		124	-

The real test for MHz defibrillation is, however, whether the average voltage and energy improve on that of long shocks of the same duration. The average threshold for the pulse trains is 19 ± 1.6

V/cm, while for the single shock it is 22 ± 1.5 V/cm. There is no statistically significant difference in these thresholds ($p = 0.17$). However, when comparing the percentage difference in defibrillation threshold for pulse trains compared with the long shock for each heart, it comes out to -13 ± 5%. Using a one sample t-test where the expected mean is 0, this result is significant ($p = 0.0375$). This indicates that while there is variation between hearts, the pulse train consistently has a slightly lower average threshold than the single millisecond shock.

The threshold energies were calculated, with a mean of 756 ± 160 mJ for the pulse trains and 581 ± 120 mJ for single shocks ($p =0.4089$). When the percentage difference in energies for each heart is compared, the pulse trains require 43 ± 27% more energy to defibrillate than the millisecond shocks. This difference is statistically significant ($p = 0.0241$).

The electric field threshold for 5+5 ms biphasic shocks (9.7 ± 0.3 V/cm) is much lower than either the pulse train, or monophasic shock. Energy calculations were only possible in one instance, however, the defibrillation energy is much lower for biphasic (299 mJ) compared with monophasic (519 mJ) or the pulse train (1150 mJ).

6.2.2 Success Curves

Since the transition between unsuccessful and successful defibrillation attempts is not a sharp cutoff, the success rate for each pulse condition in all hearts is shown in Figure 21. Since exact voltages were not applied for every defibrillation attempt, the electric field values were grouped for each pulse condition.

The success rate as a function of electric field has been fitted by a sigmoidal curve for each of the shock types (see Fig. 20). The following equation was used for the fitting:

$$SR = \frac{1}{1+e^{-(E-ED50)/n}}$$ Equation 8

Where *SR* is the success rate, *E* is the electric field, *ED50* is the electric field at the point of inflection, and *n* is a measure of steepness.

While monophasic and biphasic shocks exhibit a sharp transition from failed defibrillation to successful defibrillation as the field strength is increased, the transition for MHz trains is more extended.

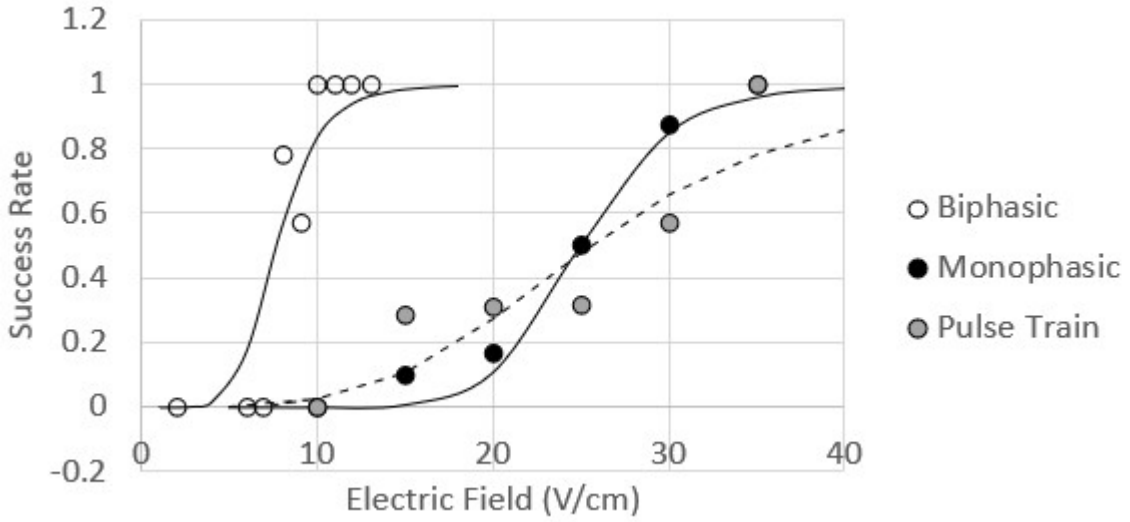

Figure 21. Success rate of defibrillation for increasing electric field strength. Biphasic shocks have a more clearly defined transition between successful and unsuccessful attempts, whereas the MHz pulse train (dashed line) and monophasic shocks have a more gradual transition. The electric field for the MHz pulse trains is the average electric field. Since the shock electric field is on a continuum, the data is binned, with a bin size of 2 for biphasic shocks and 5 for monophasic shocks and MHz trains. Each data point on the graph represents a minimum of 2 and a maximum of 22 attempts, except for 35 V/cm for the pulse train, which is a single data point. The total number of shock applications is 28 for biphasic, 58 for monophasic, and 66 for the pulse trains.

For the biphasic shocks, the ED50 is 7.7 and n is -6.2 ($R^2 = 0.89$). For monophasic shocks, ED50 is 25.0 and n is -9.5 ($R^2 = 0.99$), and for the pulse trains, ED50 is 25.5 and n is -4.0 ($R^2 = 0.81$). Thus, for all shock modalities, the fit line reasonably well predicts the relationship between electric field and success rate. The ED50 for the monophasic shocks and the pulse trains is very similar while the ED50 for the biphasic shocks is much lower, which is to be expected.

6.2.3 Electrophysiological effects of MHz defibrillation

The action potential duration (APD) of cases where a defibrillation shock induced an action potential were analyzed for bipolar shocks, monopolar shocks, and MHz pulse trains. If defibrillation was delayed, the APD of the first full beat was analyzed. The difference in the action potential induced by the defibrillation shock and the subsequent sinus beat was then compared with the difference between the two sinus beats immediately following the defibrillation shock. Averaged over seven hearts (n = 9 for MHz, 8 for MP, and 5 in 4 hearts for BP), the difference between the induced APD and following APD was 10.5 ± 3.3% (p = 0.01) for MHz, 22.2 ± 6.2% (p = 0.01) for MP, and 22.2 ± 3.5% (p = 0.003) for BP. P-values were calculated using a one-sample t test with a null hypothesis of 0%. The difference between the two post-shock sinus beats was -4.5 ± 2.5% (p = 0.1) for MHz, -4.2 ± 2.9% (p = 0.2) for MP, and -3.5 ± 4.6 % (p = 0.5) for BP. For all shocks the shock-induced APD was slightly shorter than the following shock. However, the difference between the two sinus beats was negligible, signaling that the effects of the defibrillation shock are transient.

The diastolic interval (DI) is the duration between the end of one action potential and the beginning of the next action potential. The DI immediately after a defibrillation strength shock

was compared with the following DI. Additionally, the second and third post-shock diastolic intervals were also compared. These analyses were performed for seven hearts (n = 9 for MHz, 8 for MP, 4 in 4 hearts for BP) and averaged. The percentage difference between the first two post-shock diastolic intervals was 35.5 ± 5.2% (p = 0.0001) for MHz, 31.9 ± 4.6% (p = 0.0002) for MP, and -25.5 ± 4.1 % (p = 0.008) for BP. The difference between the second and third post-shock sinus beats was 3.6 ± 2.8% (p = 0.2) for MHz, 0.7 ± 1.1% (p = 0.5) for MP, and 2.8 ± 3.4 % (p = 0.5) for BP. Thus, for all pulse conditions, though there is a significant increase in the diastolic interval following a defibrillation-strength shock, the effect appears transient, as there is no difference between the following diastolic intervals. This behavior was also observed for 300 ns, but the increase in diastolic interval observed here is much smaller than that seen for 300 ns defibrillation shocks which had an increase of 58.9%.

Additionally, no change in baseline was observed for any defibrillation shocks, indicating that there was no electroporative damage in the tissue.

6.2.4 Modeling Analysis

To help visualize what is happening at the cell membrane for the pulse train and single long shock, the charging and discharging equations for an RC circuit were used to create a model in MATLAB. Using the charging time constant from the best fit for the stimulation strength-duration curve (200 μs), it is possible to model the charging behavior of the long shock and MHz pulse train (see Figure 22).

The applied electric field of the long shock was chosen to be 1 for simplicity, which is taken to be the threshold for defibrillation. According to the stimulation strength-duration curve from

Chapter 5, the 2.5 ms pulse duration falls in the regime of rheobase, where a minimum voltage is required for stimulation, no matter how long the shock becomes.

In our experimental results, the threshold voltage for MHz defibrillation was 1.85 times that required for the long shocks, so 1.85 is the pulse train voltage selected for the model. The average voltage of the experimental waveform was approximately half of the total, so a duty cycle of 47.5% was used with a repetition frequency of 0.4 MHz. The charging time constant was initially set to $\tau = 200$ μs. For all conditions, the time constant when the external stimulus was removed was 200 μs since the cell membrane has no memory of what field was applied previously.

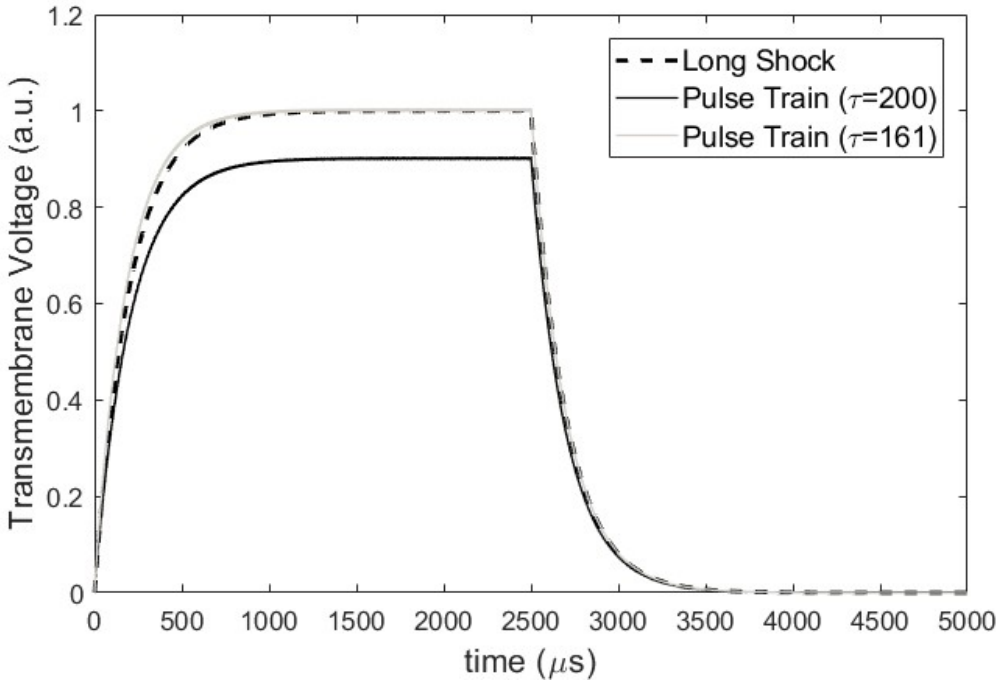

Figure 22. Model membrane charging in response to a single 2.5 ms shock with τ = 200 μs (dashed line), the pulse train of 1000, 1000 ns shocks at 0.4 MHz with τ = 200 μs (black line), and the pulse train with τ = 171 μs (grey line).

The model results showed that the MHz pulse train resulted in membrane charging that did not reach the threshold for defibrillation (10% below) while in the corresponding experiments, we do see defibrillation for the modeled pulse conditions. This shows that nanosecond shocks are slightly more effective than predicted by our model. One explanation could be that charging becomes quicker for higher amplitude shocks. This would be consistent with results by Efimov which show that the time constant decreases with an increase in voltage for 8 ms defibrillation shocks [55].

When the time constant during charging is decreased (the discharging time constant is kept at 200 μs), the maximum transmembrane voltage increased. The results with a 19.5% smaller charging time constant (161 μs) most closely matched with the charging behavior of the single long shock. Thus, it is possible that the charging time constant decreases slightly for the MHz pulse train. However, there could also be error in the model due to the assumption of a perfectly square waveform for the applied voltage.

6.3 Discussion

In our experiments, the electric field threshold for defibrillation with the MHz pulse trains was, much lower than the stimulation threshold for a single 1000 ns shock as determined in Chapter 5. Additionally, the average threshold electric field of the MHz pulse trains was consistently lower than for the 2.5 ms shocks, though the threshold energy for MHz pulse trains was almost twice that of the longer shocks.

Optical mapping trace analysis revealed that the heart behaves similarly for all pulse conditions, with the defibrillation shock resulting in a slightly shorter than average action potential duration

as well as an extended diastolic interval. Both of these changes were transient, and after a subsequent sinus beat, there was no detectable difference in either action potential duration or diastolic interval.

6.3.1 Energy Comparison

Thus, while the average electric field for the nanosecond pulse trains was slightly lower, the energy requirement was 43% higher. This is consistent with what we expect when doubling the electric field amplitude for the pulses. Energy is calculated by integrating the product of the current and voltage. In a primarily resistive load, such as the heart perfused with Tyrode's solution, the current is equal to the voltage divided by the resistance, making energy proportional to the square of the voltage. Thus, if the electric field is doubled, energy is multiplied by a factor of four. However, the total "on" duration is only half, and since energy is power integrated over time, the expected energy difference between the long shock and the pulse train is approximately 50%, consistent with the results seen above.

6.3.2 Comparison to results in cells

The result that MHz pulse trains require lower electric fields to defibrillate is consistent with those seen in nerves and cells. Pakhomov et al. showed that it is possible to excite and electroporate cells using a pulse train of nanosecond shocks of much lower amplitudes at MHz frequencies [38]. For trains of 5 and 100 shocks of 340 ns duration, the amplitude required for nerve stimulation decreases at pulse repetition frequencies above approximately 5 kHz. For 100, 200, and 400 ns shocks, the time-averaged nerve stimulation amplitude depends only on the burst duration and is independent of the individual shock duration. For a burst of 100 shocks of 200 ns

duration at 3.3 MHz, the time averaged stimulation threshold is the same as the threshold for a 300 μs shock that is the same duration as the pulse train. This is consistent with what we see for MHz defibrillation, where the time-averaged electric field threshold is similar for the pulse trains and the single 2.5 ms shock.

In cardiomyocytes, MHz compression is also effective in reducing the stimulation electric field threshold [38]. Interestingly, when the stimulation threshold time-averaged electric field is plotted against burst duration, there is a decrease for shorter pulses. This effect was not seen in nerves and indicates that shorter nanosecond shocks affect cardiac cells and tissues than longer shocks. Using shocks shorter than 1000 ns may allow us to decrease energy and electric field thresholds.

6.3.3 Implications

The electric field reduction of MHz pulse train defibrillation matches well with results seen in other excitable cells. A possible explanation has already been introduced in Section 5.3.1. For millisecond shocks, defibrillation with higher amplitude shocks results in faster time constants [55]. Thus, it is possible that the lower than expected energy of nanosecond defibrillation described in Section 3.3.2 is due to the high fields required. However, the MHz pulse train still requires more energy to defibrillate than a long millisecond shock. The threshold electric field is much lower than that for 300 ns, and the greater effectiveness of higher amplitudes is balanced out by the higher energy required for higher electric fields.

6.4 Conclusion

MHz compression defibrillation is possible with no lasting electrophysiological side effects. The average electric field of the pulse train is slightly lower (13%) than for a single defibrillation shock of the same duration, though the energy required is 43% higher. Modeling analysis shows that increasing the time constant explains the lower electric field for the pulse train, though this increase is not sufficient to decrease the energy to levels comparable to the long shock.

CHAPTER 7:

60 NS DEFIBRILLATION AND STIMULATION

7.1 Introduction

Since 300 ns defibrillation exhibited a dramatically reduced defibrillation threshold energy, it is an intriguing question if the use of even shorter nanosecond defibrillation shocks could potentially defibrillate at even lower energies. It has been demonstrated that stimulation of excitable cells is possible with shocks as low as a few nanoseconds. In chromaffin cells, 5 ns shocks are able to stimulate the cells, causing Ca^{2+} entry which triggers catecholamine release [39]. In nerves, 12 ns stimulation is possible without electroporative damage [27]. Shorter, nanosecond shocks could possibly result in less electroporative damage in addition to lower energy. 60 ns shocks are almost an order of magnitude shorter than the previously tested nanosecond defibrillation shocks.

A 60 ns transmission line pulse generator was first designed and tested. The defibrillation thresholds and energies of 60 ns and 5+5 ms biphasic shocks were then compared to determine whether or not these short nanosecond shocks are more efficient at terminating fibrillation than the current, clinically implemented defibrillation technology. The defibrillation threshold for 60 ns shocks turned out to be significantly higher than predicted. The pulser we designed could not produce the higher amplitude required, but successfully defibrillated with a pair of 60 ns shocks. This data enabled us to estimate the upper and lower bounds for the 60 ns defibrillation threshold.

Additionally, bipolar cancellation has been studied in various cell types [40, 41]. Bipolar cancellation occurs when a second, negative phase of a nanosecond waveform cancels the response to the positive phase. Of particular interest is the possibility that by choosing appropriate wave forms, cancellation itself could be cancelled in parts of space, which would allow the delivery of a stimulus far from the electrodes, with the result closer to the electrodes being cancelled [68]. If this technology is realized on a larger scale, it could result in the replacement of implantable defibrillators and pacemakers with ones external to the body, or allow us to minimize shock effects on tissues for external defibrillation. Thus far, bipolar cancellation has not been demonstrated in tissues other than nerves. Thus, we investigated 80 ns shocks with a second, negative phase of varying amplitude (-15% and -29%) and looked for differences in their stimulation threshold.

7.2 Results

7.2.1 Pulser design and testing

A transmission line pulse generator was designed to supply shocks of 60 ns duration. In order to achieve impedance matching, the impedance of our experimental setup of parallel plate electrodes submerged in Tyrode's solution with a heart in between was determined to be approximately 15 Ω. RG-58 cables with an impedance of 50 Ω were selected, so we used multiple cables in parallel to achieve impedance matching. Four cables in parallel resulted in a pulser impedance of 12.5 Ω, while using 3 cables resulted in 16.7 Ω. Thus a three-cable pulser design was chosen.

Upon initial testing, the resulting waveform was almost twice as wide as designed and there were significant oscillations and an up to 40% negative phase after the initial positive phase (see Figure 23). Since the impedance was fairly well matched, this was likely due to inductance in the wires between the pulser and the electrodes. Inductance between two parallel wires is given by

$$L_{wires} \approx \frac{\mu_0 \mu_r L}{\pi}\left[\ln\left(\frac{S}{D}\right) + \frac{1}{4}Y\right] \qquad \text{Equation 9 [69]}$$

Where μ_0 is vacuum permeability, μ_r is the relative permeability of the insulator between the wires, *S* is the spacing between the conductors, *D* is the conductor diameter, *L* is the length of the conductor, and Y denotes the distribution of current in the wire, with 0 indicating that current flows only on the surface, and 1 indicating that the current is evenly spread over the cross-section. So to decrease the inductance, the length of the wires was halved from approximately 3 feet to 1.5 feet. This slightly improved the waveform, though the pulse duration was around 80 ns and there was still a significant negative phase.

For a coaxial cable, the inductance is given by

$$L_{coaxial} \approx \frac{\mu_0 \mu_r L}{2\pi} ln\left(\frac{D}{d}\right) \qquad \text{Equation 10 [70]}$$

Where *D* is the outer diameter of the coaxial cable and *d* is the inner diameter of the coaxial cable. Assuming that the ratio of *S/D* for the parallel wires and *D/d* for coaxial cable is 2, Y is 0, and the lengths and relative permeabilities are the same, a coaxial cable has about half the inductance of the parallel wires. However, using three coaxial cables to transmit the pulse from the pulser to the electrodes minimized the distance the signal has to travel through the wires which contribute to stray inductance, which improved the waveform as seen in Figure 23.

Even with these steps, there was still a negative phase, thus a high power diode was placed in parallel to the load to shunt the current of the negative phase, to give the best waveform with a full width half maximum (FWHM) pulse duration of 60 ns.

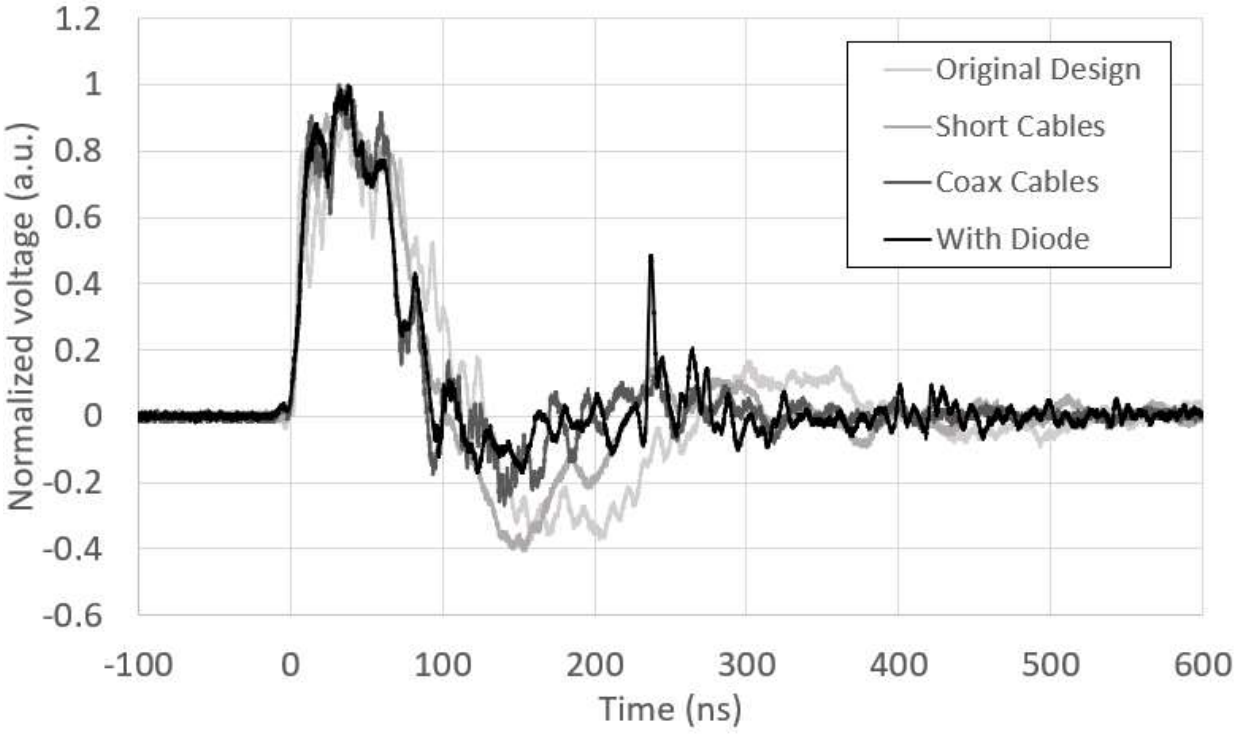

Figure 23. Representative waveforms of various delivery methods for the 60 ns pulser. All voltage waveforms are normalized to the maximum voltage in order to better compare the pulse shape. The lightest grey trace shows the waveform when two insulated, twisted wires are used to connect the pulser to the electrodes placed on either side of the heart. The next lightest trace is the result of shortening the two wires from approximately 3 ft to 1.5 ft. The next darkest trace is when the twisted wires are replaced with three parallel coaxial cables, and the black waveform results from the coaxial cables and a high power diode being placed in parallel in order to shunt the negative current.

For bipolar cancellation experiments, the second lightest grey waveform from Figure 23 was used, with short, twisted cables connecting the pulser to the electrodes, and compared with the waveform produced by the same pulser setup, with a diode in series (see Figure 24). Measured by taking the ratio of the minimum to maximum voltage, the waveforms have a negative phase of 15 ± 2% (with diode) and 29 ± 3% (without diode). The duration of the negative phase is 80 ns (FWHM) for the -29% waveform and slightly shorter for the -15% waveform at 50 ns (FWHM).

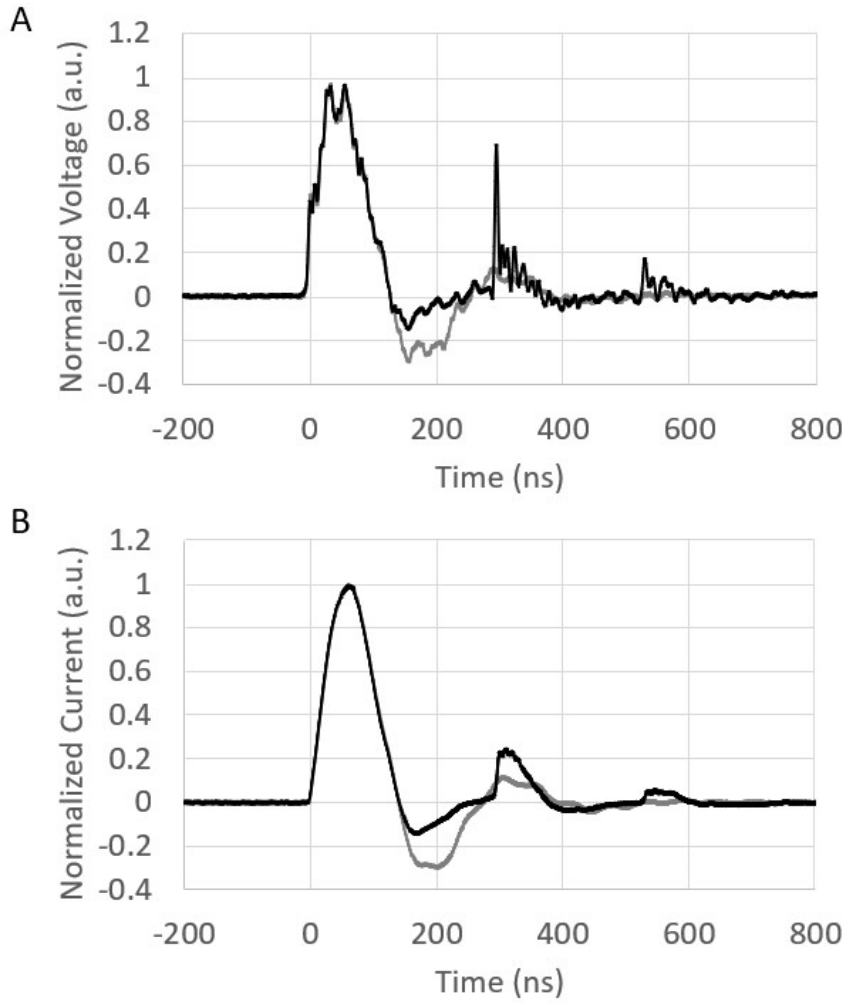

Figure 24. Waveforms used for bipolar cancellation experiments. The black traces show the voltage (A) and current (B) when a high power diode is placed in parallel with the load to shunt the negative current. The grey traces show voltage and current when the diode is removed.

There was a spike in the voltage waveform when the diode is placed in parallel. However, this was not nearly as prominent in the current waveform, indicating it might be a recording artefact. Additionally, the energy deposition after the negative phase is only 1% of the total for the -29% waveform and 3% of the total for the -15% waveform. These values are small enough compared to the effects of both positive and negative phases that they can be disregarded.

7.2.2 Stimulation

Stimulation with 60 ns shocks was attempted in 3 hearts with an average stimulation threshold of 2.46 ± 0.12 kV/cm. This allows for the extension of the stimulation curve shown in Figure 19, the nanosecond regime of which is replicated below with the 60 ns data point added. This value is almost twice as high as predicted by the -0.75 slope determined in Chapter 5, which predicts a stimulation threshold of 1.3 kV/cm (see solid line in Figure 25).

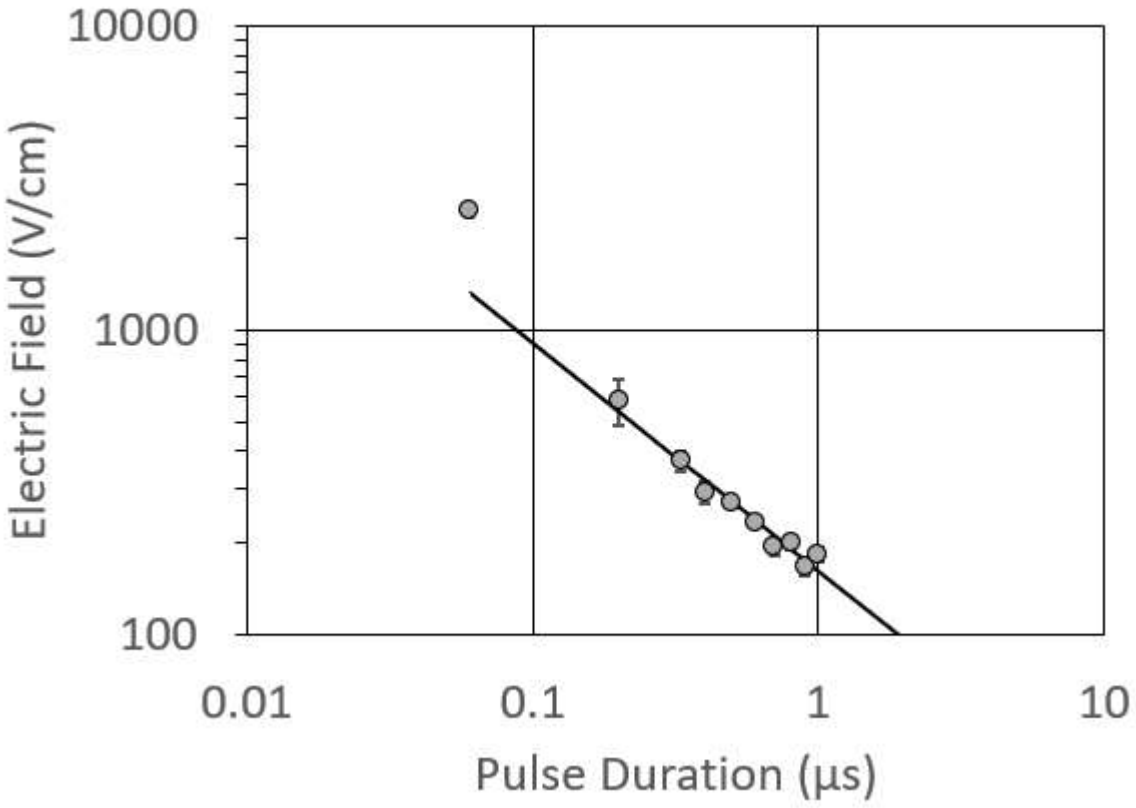

Figure 25. The stimulation strength-duration curve extended to 60 ns. The circles indicate the experimentally determined stimulation electric field thresholds. The trend line for 200-1000 ns shocks is displayed (black).

7.2.3 Defibrillation

During initial experiments, defibrillation with a single 60 ns shock was not possible since we achieved a maximum electric field of only 4.8 kV/cm. In four fibrillating hearts, 12 shocks above 4.5 kV/cm were applied without resulting in defibrillation. Technical limitations of the pulser and optical mapping setup prevented us from increasing the field even farther. A test shock above this maximum caused the computer and the camera to stop responding. Thus, we can say the lower bound for the defibrillation threshold is around 4.5 kV/cm.

In two instances, we exposed to tissue to pairs of pulses, when the pulser fired two shocks in rapid succession, and these instances resulted in defibrillation (see Figure 26). In both cases defibrillation was slightly delayed, approximately 400 ms after the last shock application. However, this delay is commonly seen for defibrillation shocks close to the threshold [71, 72], and since fibrillation was sustained for 30 seconds before the defibrillation shock, it is unlikely that it would terminate spontaneously. The thresholds were 3.84 and 3.95 kV/cm, very close to the maximum achievable electric field. Thus, 60 ns shocks are capable of defibrillating.

To obtain a better estimate of the defibrillation threshold, we took the stimulation threshold for 60 ns, assuming that the ratio of stimulation and defibrillation remains constant, and used the results for 300 ns to approximate the defibrillation threshold for 60 ns. The defibrillation threshold determined for 300 ns shocks was approximately twice that of the stimulation threshold. If this relationship holds true for the 60 ns shocks, the defibrillation threshold should be approximately 5 kV/cm. This translates to 7.5 kV for an electrode spacing of 1.5 cm, which is larger than the pulser is capable of producing.

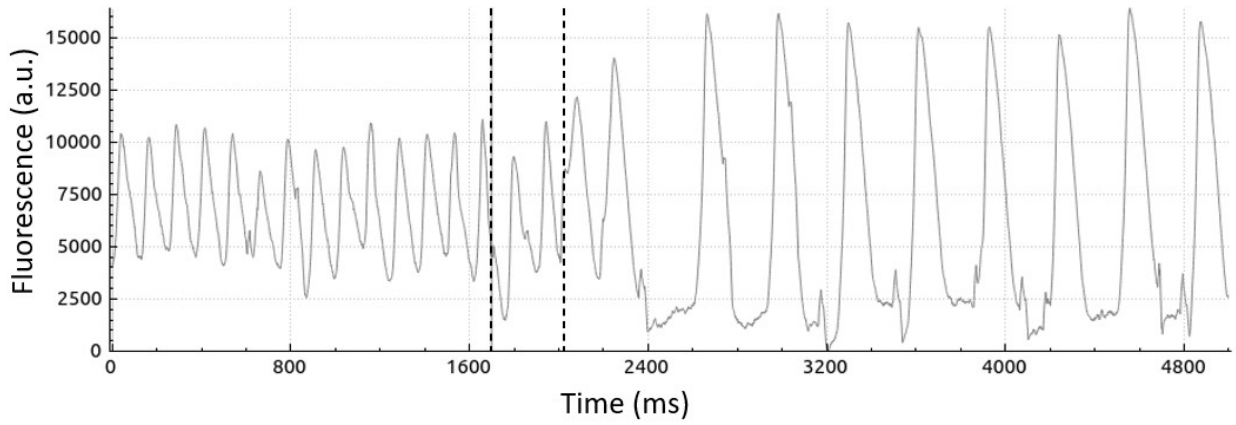

Figure 26. Example of two 60 ns shocks terminating fibrillation. The red lines indicate shock placement. Defibrillation is delayed slightly after the second shock is applied.

As discussed in previous chapters, we also analyzed the energy required for defibrillation with 60 ns shocks. Only the second of two shocks was captured by the oscilloscope, but an approximation of the total defibrillation energy can be obtained by doubling the energy of the single shock. The energy of the second shock was 268 and 273 mJ in the two hearts for which we observed defibrillation with a pair of shocks. Double this amount would be almost 550 mJ per defibrillation instance. Assuming the heart is mainly a resistive load, the energy is proportional to the square of the electric field. Thus, 5.6 kV/cm is an upper bound for the defibrillation threshold, though it is likely much less since the membrane will discharge between shock applications.

In three hearts, including the two in which defibrillation was achieved with two 60 ns shocks, the defibrillation threshold for 5+5 ms biphasic shocks was determined. Both phases were not always the same amplitude due to the use of a different power supply for each phase. However, the negative phase was typically within 3-5 V of the positive phase. Thus the minimum electric field for defibrillation for the three hearts was averaged over all 6 phases to give a threshold of

16 ± 0.6 V/cm. The average energy at the threshold is 724 ± 9 mJ. Notably, this is more than the energy of the double 60 ns shocks which achieved defibrillation.

7.2.4 Bipolar cancellation

Bipolar cancellation has been observed in cells [40, 73] and nerves [41]. In nerves, bipolar cancellation was found to be stronger for shorter shocks. The 60 ns pulser can be set up to have a negative phase, which can mostly be removed by the addition of a diode in parallel to shunt the negative current. Thus, the stimulation thresholds of shocks with a 29% negative phase and a 15% negative phase were determined. See Figure 24 for voltage waveforms. The pulse duration was slightly broader than previously and is approximately 80 ns.

Stimulation thresholds were determined repeatedly for four hearts. The stimulation threshold increased slightly with time in setup (see Figure 27). However, the trend was linear, and a line of best fit for each of the pulse conditions shows a clear separation on the range of approximately 100-200 V/cm.

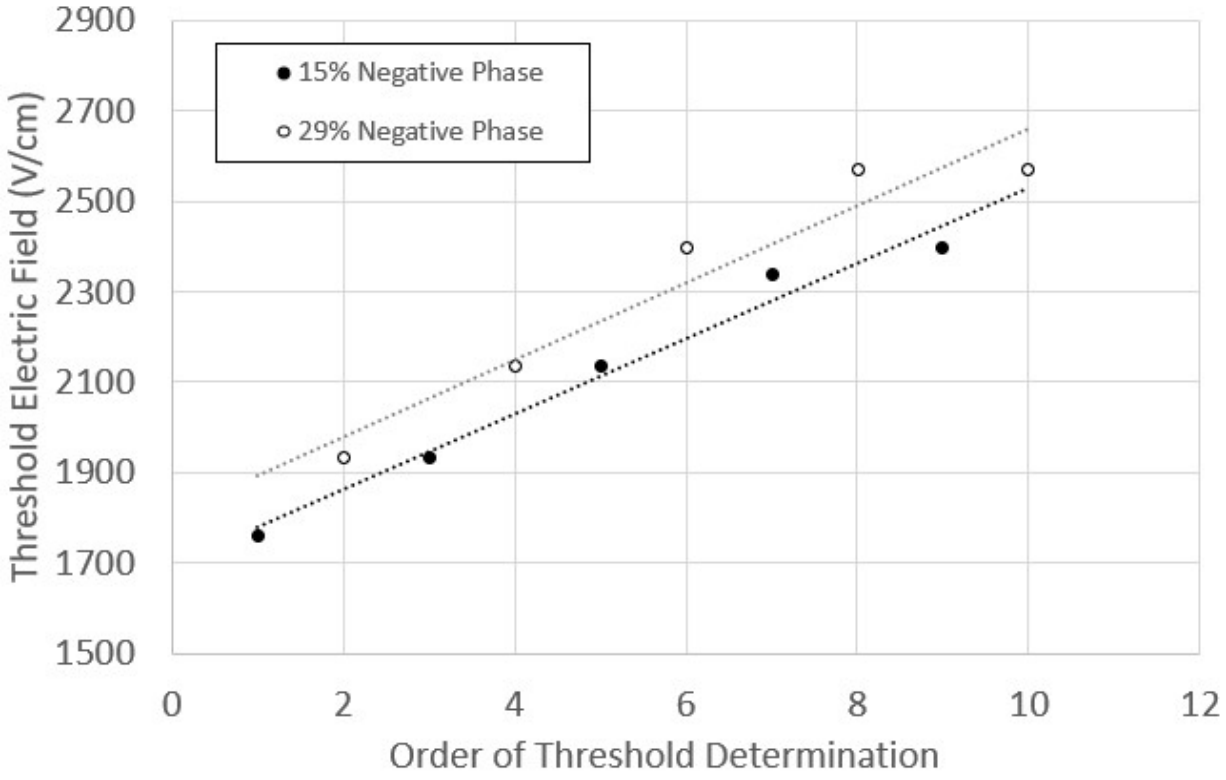

Figure 27. Threshold for 80 ns shocks with a 15% (black) and 29% (white) negative phase in a representative heart. The horizontal scale represents the order in which the thresholds were determined. The line of best fit for each is also displayed.

Taking the trend lines for all four experiments, and comparing each data point with the trend line of the other pulse condition, there is an average difference of 124 ±15 V/cm, which is statistically significant compared to a null hypothesis of zero ($p = 0.0001$). This translates to a 5.6 ± 0.7% increase in the threshold of the -29% waveform in comparison to the -15% waveform.

When comparing the energy of the stimulation thresholds for the two waveforms, a similar separation was noted, with the -29% waveform requiring less energy that the -15% waveform. The average difference is 23.5 ± 2.8 mJ ($p = 0.0004$) which is an increase of 17.6 ± 1.8% over

the -15% waveform. Thus, the separation in the energy required for stimulation is even greater than the voltage.

7.2.5 Electrophysiological Effects

The diastolic interval following the two applied defibrillation shocks was an average of 81 ± 45% longer than the subsequent DI. The difference in the second and third post-shock DI is 6.7 ± 9%. Unfortunately, not enough defibrillation events occurred to draw statistical conclusions, but it seems that there is an extended diastolic interval immediately post shock similar to that observed for the other defibrillation modalities presented in Chapters 3 and 6.

Stimulation-strength shocks also display a prolonged post-shock DI (4 hearts, n=15). The first post-shock DI is 31 ± 4% longer than the diastolic interval immediately preceding the stimulation shock. The subsequent DI returns to normal, being an average of 0.4 ± 1.3% of the pre-shock DI. Thus, as for defibrillation-strength shocks, the increase in diastolic interval is temporary and not indicative of lasting damage. Additionally, there is no difference in the change of the post-shock DI when comparing the bipolar shocks with 15% and 29% negative phase.

The action potential durations for the 80 ns bipolar stimulation shocks were compared with that of sinus beats (4 hearts, n=15). There was a slight decrease in action potential duration for the shock-induced beat, which was 2.45 ± 0.8% ($p=0.01$) shorter than the previous sinus beat. However, the post-shock beat APD was 1.21 ± 0.7% ($p=0.13$) of the pre-shock APD. There was no difference in the response to the 15% and 29% waveforms.

All traces for both defibrillation and stimulation were analyzed for traces of baseline shift, which would indicate electroporation, but none was evident.

7.2.6 Tissue Damage

Notably, though the stimulation threshold increased over time, we were able to apply hundreds of 80 ns shocks within 50% of the threshold. Over four experiments, an average of 211 ± 17 stimulation events were documented. This is actually an under-representation of the number of shocks to which the heart was exposed, since at least twice as many shocks were recorded but not saved due to application during the refractory period of the previous sinus beat. Experiments were ended after the internal pressure at the aortic cannula exceeded 120 mmHg even with the flow rate reduced to 10-15 mL/min, or the heart no longer sustained a sinus rhythm.

7.3 Discussion

We have shown that 60 ns defibrillation is possible, as evidenced by the two instances where two shocks achieved defibrillation. Due to the limitations of our setup, we were not able to achieve defibrillation with a single shock. However, we were able to extrapolate the upper bound of the single shock defibrillation threshold to be around 5.6 kV/cm, with a lower bound of 4.5 kV/cm.

7.3.1 Stimulation threshold

The stimulation threshold determined for 60 ns was 2.46 ± 0.12 kV/cm, almost double that predicted by fitting the strength-duration curve determined in Chapter 5. However, there was still a 13% negative phase for the 60 ns waveform. Since the shock was not entirely monophasic, it is possible that biphasic cancellation occurs as in nerves and other cells [41, 73, 74], which would indicate that the true stimulation threshold is somewhat lower.

In studies in nerves, bipolar cancellation was stronger for shorter shocks, with even a 10% negative phase resulting in approximately 35% reduction in compound action potential amplitude for 200 ns shocks [41]. For a 20% negative phase, almost 80% reduction in amplitude was observed. These studies do not analyze the difference in thresholds different waveforms, but for higher amplitudes, even the shocks with a negative 20% phase should stimulate as normal. If this pattern holds true for 60 ns shocks in cardiac tissue, the small negative phase could account for at least part of the discrepancy between the predicted and actual stimulation thresholds, though likely not all.

Additionally, in murine ventricular cardiomyocytes exposed to 10, 800 ns shocks at a frequency of 5 Hz, a 50% negative phase reduced propidium iodide uptake by almost 60%, while a 25% negative phase caused a reduction of around 50%, compared with monopolar shocks [40]. For 400 ns shocks, the reduction is even greater, with a 50% negative phase causing a reduction of almost 25% in PI uptake. Thus, since similar trends are observed for cardiomyocytes as for nerves, it is likely that bipolar cancellation occurred for our stimulation shocks, and the threshold for an ideal monopolar 60 ns shock could be closer to that predicted by the strength duration curve of Chapter 5.

If the stimulation threshold for true 60 ns monopolar shocks is consistent with the strength-duration curve of other nanosecond shocks, it is likely that similar mechanisms are responsible for depolarizing the cell membrane to the stimulation threshold. As Chapter 5 suggests, membrane charging via the motion of ions is likely the primary mechanism, though a secondary mechanism such as electroporation or electropermeabilization is likely responsible for a portion of the response.

7.3.2 Bipolar cancellation

Bipolar cancellation was observed for our shocks with a 15% and 29% negative phase, with the 30% negative phase requiring an electric field approximately 6% higher to stimulate. This is a fairly small difference, though statistically significant. A comparison with a true monophasic shock would likely give a much larger difference.

All the cancellation studies mentioned here keep the amplitude of the first phase constant while varying the second phase. Our experiments vary both simultaneously. Thus it is unknown how large an increase in total stimulus amplitude is required to achieve the effects of a monophasic shock or one with a smaller negative phase. Thus, our study is the first to show an increase in stimulation threshold with an increase in the negative phase of a bipolar shock.

Though bipolar cancellation has been observed in cells and nerves, this study is the first demonstration of cancellation in a larger tissue or organ and it supports further research into remote stimulation or defibrillation using “cancellation of cancellation” to minimize electric field effects close to the electrodes.

7.3.3 Safety Concerns

We were not able to achieve defibrillation with a single 60 ns shock. The power supply was grounded to the optical table upon which all the acquisition hardware (acquisition board, computer, camera) rested. The highest shock we applied (4.8 kV/cm at the electrodes) caused the computer and camera to temporarily stop functioning, though restarting both restored normal functionality. Even stimulation-strength shocks always resulted in acquisition malfunction, causing inversion and translation of sections of the optical mapping recording. The effect on the

system was temporary, though the changes persisted through the end of the recording. Subsequent recordings had normal video orientation until shocks were applied. Thus, if 60 ns defibrillation were to be used on a patient with blood pressure, pulse oxygen, or other monitors, it is possible malfunction could occur. External paddle electrodes would require even higher voltages, and electrical side effects could be an even greater concern. However, electromagnetic shielding of monitors or around the pulser and electrodes could mitigate this problem.

7.4 Conclusion

In conclusion, though 60 ns defibrillation is possible, though higher voltages are required for single shock defibrillation than were tested here. However, the high voltages required create numerous technical and safety issues, though they could be mitigated using electrical shielding. The stimulation threshold is higher than that predicted by the strength-duration curve in Chapter 5, though this discrepancy is likely accounted for by bipolar cancellation. When comparing the stimulation thresholds of two 80 ns shocks with a 15% and 29% negative phase, the latter requires a 6% higher electric field to stimulate, indicating that bipolar cancellation does indeed occur in cardiac tissue.

CHAPTER 8:

CONCLUSIONS

8.1 Conclusions

In Chapter 3, we showed that 300 ns defibrillation is possible with energy lower than 10 ms conventional defibrillation by almost an order of magnitude. Aside from a temporary increase in the diastolic interval, there was no sign of tissue damage in the optical mapping traces. Additionally, histological analysis showed no sign of electroporation or tissue death. This work demonstrated the viability of nanosecond defibrillation as an alternative to conventional defibrillation.

Chapter 4 explored the safety of 300 ns defibrillation in more detail. Cardiac tissue damage from electric shocks was assessed using needle electrodes that caused only local damage and allowed 10-15 applications per heart. Using numerical modeling, the electric field distributions for the needle electrodes were be related to those of a parallel plate geometry typically used for defibrillation. The safety factor, i.e. the ratio of damage threshold and the defibrillation threshold, of nanosecond defibrillation was in the range 5-7, similar to that of millisecond defibrillation. This confirmed the potential of nanosecond defibrillation as a low-energy alternative to conventional defibrillation.

The stimulation strength-duration curve for cardiac tissue was extended down to 200 ns in Chapter 5. Stimulation with nanosecond shocks was shown to be repeatable with no change in action potential duration or shape over the course of an experiment. At shorter pulse durations, there was a deviation of the curve from that predicted by membrane charging which could be

explained be either faster charging time constants due to higher electric fields or electroporation before stimulation.

MHz compression was explored in Chapter 6, with the result that the average electric field required for defibrillation was slightly lower than for a single shock of the same duration, though the energy was higher. No permanent electrophysiological changes were observed. The results indicated that the reduction electric field and energy thresholds of nanosecond shocks when compared with longer shocks is due to the high amplitude rather than the short timescale, since the reduction in energy for 300 ns shocks compared to 10 ms shocks was not seen for the MHz pulse train and 2.5 ms shocks, though there was a slight decrease in the electric field.

Finally, 60 nanosecond defibrillation and stimulation were tested. A single 60 ns shock was not able to defibrillate at up to 4.8 kV/cm, the maximum field strength our pulser could provide. We did, however, estimate the upper bound for the defibrillation threshold at 5.6 kV/cm using results from defibrillation with pairs of 60 ns shocks. The optical mapping traces observed were comparable to findings reported for the other nanosecond defibrillation modalities. When stimulation with a negative, second phase of varying amplitude was tested, bipolar cancellation was observed. These results are broadly consistent with those seen in other excitable cells.

In summary, this work is an exploration of the efficacy, safety, and feasibility of nanosecond defibrillation. 300 ns defibrillation shows the most promise, with a large observed energy reduction from 10 ms shocks. Studies to determine the safety factor indicate that nanosecond defibrillation is at least as safe as millisecond defibrillation. MHz defibrillation requires higher energy to defibrillate than a single, long shock of similar duration, though the average voltage is slightly lower. Decreasing the duration of the individual shocks could possibly improve the

results for MHz defibrillation. 60 ns defibrillation is limited by the electrical effects of the shock on the recording system, though experiments in 60 ns bipolar cancellation seem to indicate that membrane charging occurs similarly to longer shocks. Finally, the stimulation strength-duration curve suggests a secondary mechanism to membrane charging, likely electropermeabilization at high voltages. Whether this is caused by nanoelectroporation of the cell membrane or interactions with some existing ion channel or other membrane component remains to be determined.

VITA

Johanna Neuber, B.S.E.E., M.S.E.C.E.

Email: juneuber3@gmail.com, Phone: (806) 470-0443, 940 W Princess Anne Rd #5A, Norfolk, VA 23507

EDUCATION

The University of Texas at Austin
B. S. in Electrical Engineering with a Biomedical Concentration *May 2014 (GPA: 3.82, with Honors)*
Minor in German

Old Dominion University
M. S. in Electrical and Computer Engineering *May 2016 (GPA: 3.96)*
Ph. D. in Biomedical Engineering *Expected Graduation: December 2020*

AWARDS

2019 World Congress on Electroporation Student Presentation Award
Won 200 Euros for 3rd place student presentation in the Biomedical Engineering category

2019 ISEBTT Student Travel Award
Received a travel grant of $1,000 to attend the World Congress on Electroporation

2017-19 American Heart Association Predoctoral Fellowship
Received funding ($31k per year for 2 years) to determine the mechanism of nanosecond defibrillation

2015 BioCAS Student Attendance Award
National Science Foundation division of Electrical, Communication, and Cyber Systems

2015 M.S.E.E. Graduate Researcher Award
Old Dominion University Department of Electrical and Computer Engineering

PUBLICATIONS

Journal Publications (selected)

1) J.U. Neuber, A.G. Pakhomov, C.W. Zemlin, "Electroporation safety factor of 300 nanosecond and 10 millisecond defibrillation in Langendorff-perfused rabbit hearts", PLOS ONE (under review)

2) J.U. Neuber, F. Varghese, A.G. Pakhomov, C.W. Zemlin, "Using Nanosecond Shocks for Cardiac Defibrillation", Bioelectricity (2019)

3) I. Semenov, S. Grigoryev, J.U. Neuber, C.W. Zemlin, O. Pakhomova, M. Casciola, A.G. Pakhomov, "Excitation and injury of adult ventricular cardiomyocytes by nano- to millisecond electric shocks", Scientific reports 8 (1), 8233 (2018)

4) F. Varghese, J.U. Neuber, F. Xie, A.G. Pakhomov, C.W. Zemlin, "Low-energy defibrillation with nanosecond electric shocks", Cardiovascular Research 113 (14), 1789-1797 (2017)

5) J.U. Neuber, S. Song, M.A. Malik, L. Heller, C. Jiang, "Nanosecond pulsed plasma brush for bacterial inactivation on laminate", IEEE Transactions on Radiation and Plasma Medical Sciences 1 (4), 368-375 (2017)

Conference Presentations and Manuscripts (selected

1) (**Oral Presentation at the 2019 World Congress on Electroporation**) J. Neuber, A.W. Pakhomov, C.W. Zemlin, "Electroporation Safety Factor or 300 Nanosecond Defibrillation in Langendorff-perfused Rabbit Hearts", Proc. of the 2019 World Congress on Electroporation, Septenber 3-6 in Toulouse, France

2) (**Contributed Paper at the 38th Annual International Conference of the IEEE Engineering in Medicine and Biology Society)** H. Ryan, J. Neuber, S. Song, S. Beebe, C. Jiang, "Effects of a Non-Thermal Plasma Needle

REFERENCES

[1] S. R. Gutbrod and I. R. Efimov, "A shocking past: a walk through generations of defibrillation development," *IEEE Trans Biomed Eng,* vol. 61, no. 5, pp. 1466-73, May 2014.

[2] D. J. Dosdall, V. G. Fast, and R. E. Ideker, "Mechanisms of defibrillation," *Annu Rev Biomed Eng,* vol. 12, pp. 233-58, Aug 15 2010.

[3] H. T. Truong, L. S. Low, and K. B. Kern, "Current Approaches to Cardiopulmonary Resuscitation," *Curr Probl Cardiol,* vol. 40, no. 7, pp. 275-313, Jul 2015.

[4] F. Bhanji *et al.*, "Part 14: Education: 2015 American Heart Association Guidelines Update for Cardiopulmonary Resuscitation and Emergency Cardiovascular Care," *Circulation,* vol. 132, no. 18 Suppl 2, pp. S561-73, Nov 3 2015.

[5] S. Viereck, T. Palsgaard Moller, A. Kjaer Ersboll, F. Folke, and F. Lippert, "Effect of bystander CPR initiation prior to the emergency call on ROSC and 30day survival-An evaluation of 548 emergency calls," *Resuscitation,* vol. 111, pp. 55-61, Feb 2017.

[6] P. R. Martens *et al.*, "Optimal Response to Cardiac Arrest study: defibrillation waveform effects," *Resuscitation,* vol. 49, no. 3, pp. 233-43, Jun 2001.

[7] S. Behrens, C. Li, P. Kirchhof, F. L. Fabritz, and M. R. Franz, "Reduced arrhythmogenicity of biphasic versus monophasic T-wave shocks. Implications for defibrillation efficacy," *Circulation,* vol. 94, no. 8, pp. 1974-80, Oct 15 1996.

[8] G. Ristagno, T. Yu, W. Quan, G. Freeman, and Y. Li, "Current is better than energy as predictor of success for biphasic defibrillatory shocks in a porcine model of ventricular fibrillation," *Resuscitation,* vol. 84, no. 5, pp. 678-83, May 2013.

[9] G. H. Bardy *et al.*, "Multicenter comparison of truncated biphasic shocks and standard damped sine wave monophasic shocks for transthoracic ventricular defibrillation. Transthoracic Investigators," *Circulation,* vol. 94, no. 10, pp. 2507-14, Nov 15 1996.

[10] S. J. Ley, "Cardiac Surgical Resuscitation: State of the Science," *Crit Care Nurs Clin North Am,* vol. 31, no. 3, pp. 437-452, Sep 2019.

[11] M. K. Stiles, L. Fauchier, C. A. Morillo, and B. L. Wilkoff, "2019 HRS/EHRA/APHRS/LAHRS focused update to 2015 expert consensus statement on optimal implantable cardioverter-defibrillator programming and testing," *Heart Rhythm,* May 14 2019.

[12] N. L. Gurvich and G. S. Yuniev, "Restoration of heart rhythm during fibrillation by a condenser discharge," *Am Rev Sov Med,* vol. 4, no. 3, pp. 252-6, Feb 1947.

[13] B. Lown, R. Kleiger, and G. Wolff, "The Technique of Cardioversion," *Am Heart J,* vol. 67, pp. 282-4, Feb 1964.

[14] J. S. Bradfield, E. Buch, and K. Shivkumar, "Interventions to decrease the morbidity and mortality associated with implantable cardioverter-defibrillator shocks," *Current opinion in critical care,* vol. 18, no. 5, pp. 432-437, 2012.

[15] S. C. Cook *et al.*, "Shock-related anxiety and sexual function in adults with congenital heart disease and implantable cardioverter-defibrillators," *Heart Rhythm,* vol. 10, no. 6, pp. 805-810, 2013.

[16] A. Al-Khadra, V. Nikolski, and I. R. Efimov, "The Role of Electroporation in Defibrillation," *Circulation Research,* vol. 87, no. 9, pp. 797-804, 2000.

[17] C. B. Clark, Y. Zhang, L. R. Davies, G. Karlsson, and R. E. Kerber, "Transthoracic biphasic waveform defibrillation at very high and very low energies: a comparison with monophasic waveforms in an animal model of ventricular fibrillation," *Resuscitation,* vol. 54, no. 2, pp. 183-186, 2002/08/01/ 2002.
[18] P. J. Kudenchuk, L. A. Cobb, M. K. Copass, M. Olsufka, C. Maynard, and G. Nichol, "Transthoracic incremental monophasic versus biphasic defibrillation by emergency responders (TIMBER): a randomized comparison of monophasic with biphasic waveform ascending energy defibrillation for the resuscitation of out-of-hospital cardiac arrest due to ventricular fibrillation," *Circulation,* vol. 114, no. 19, pp. 2010-2018, 2006.
[19] S. Mittal *et al.*, "Comparison of a novel rectilinear biphasic waveform with a damped sine wave monophasic waveform for transthoracic ventricular defibrillation," *Journal of the American College of Cardiology,* vol. 34, no. 5, pp. 1595-1601, 1999.
[20] Y. Zhang *et al.*, "Triphasic waveforms are superior to biphasic waveforms for transthoracic defibrillation," *Experimental studies,* vol. 42, no. 3, pp. 568-575, 2003.
[21] Y. Zhang *et al.*, "Quadriphasic waveforms are superior to triphasic waveforms for transthoracic defibrillation in a cardiac arrest swine model with high impedance," *Resuscitation,* vol. 68, no. 2, pp. 251-258, 2006/02/01/ 2006.
[22] J. Huang *et al.*, "Ascending Defibrillation Waveform Significantly Reduces Myocardial Morphological Damage and Injury Current," *JACC: Clinical Electrophysiology,* vol. 5, no. 7, pp. 854-862, 2019.
[23] R. FitzHugh, "Impulses and Physiological States in Theoretical Models of Nerve Membrane," *Biophysical Journal,* vol. 1, no. 6, pp. 445-466, 1961/07/01/ 1961.
[24] A. L. Hodgkin and A. F. Huxley, "A quantitative description of membrane current and its application to conduction and excitation in nerve," (in eng), *The Journal of physiology,* vol. 117, no. 4, pp. 500-544, 1952.
[25] I. Semenov *et al.*, "Excitation and injury of adult ventricular cardiomyocytes by nano- to millisecond electric shocks," *Scientific Reports,* vol. 8, no. 1, p. 8233, 2018/05/29 2018.
[26] W. R. Rogers *et al.*, "Strength-duration curve for an electrically excitable tissue extended down to near 1 nanosecond," *IEEE Transactions on Plasma Science,* vol. 32, no. 4, pp. 1587-1599, 2004.
[27] M. Casciola, S. Xiao, and A. G. Pakhomov, "Damage-free peripheral nerve stimulation by 12-ns pulsed electric field," *Scientific Reports,* vol. 7, no. 1, p. 10453, 2017/09/05 2017.
[28] K. H. Schoenbach *et al.*, "Bioelectric Effects of Intense Nanosecond Pulses," *IEEE Transactions on Dielectrics and Electrical Insulation,* vol. 14, no. 5, pp. 1088-1109, 2007.
[29] K. H. Schoenbach *et al.*, "The Effect of Intense Subnanosecond Electrical Pulses on Biological Cells," *IEEE Transactions on Plasma Science,* vol. 36, no. 2, pp. 414-422, 2008.
[30] T. R. Gowrishankar and J. C. Weaver, "An approach to electrical modeling of single and multiple cells," *Proceedings of the National Academy of Sciences,* vol. 100, no. 6, pp. 3203-3208, 2003.
[31] T. R. Gowrishankar and J. C. Weaver, "Electrical behavior and pore accumulation in a multicellular model for conventional and supra-electroporation," *Biochemical and Biophysical Research Communications,* vol. 349, no. 2, pp. 643-653, 2006/10/20/ 2006.

[32] A. M. Bowman, O. M. Nesin, O. N. Pakhomova, and A. G. Pakhomov, "Analysis of Plasma Membrane Integrity by Fluorescent Detection of Tl+ Uptake," *The Journal of Membrane Biology,* journal article vol. 236, no. 1, pp. 15-26, July 01 2010.
[33] A. G. Pakhomov, A. M. Bowman, B. L. Ibey, F. M. Andre, O. N. Pakhomova, and K. H. Schoenbach, "Lipid nanopores can form a stable, ion channel-like conduction pathway in cell membrane," *Biochemical and Biophysical Research Communications,* vol. 385, no. 2, pp. 181-186, 2009/07/24/ 2009.
[34] O. M. Nesin, O. N. Pakhomova, S. Xiao, and A. G. Pakhomov, "Manipulation of cell volume and membrane pore comparison following single cell permeabilization with 60- and 600-ns electric pulses," *Biochimica et Biophysica Acta (BBA) - Biomembranes,* vol. 1808, no. 3, pp. 792-801, 2011/03/01/ 2011.
[35] K. C. Smith and J. C. Weaver, "Transmembrane molecular transport during versus after extremely large, nanosecond electric pulses," *Biochemical and Biophysical Research Communications,* vol. 412, no. 1, pp. 8-12, 2011/08/19/ 2011.
[36] V. Nesin, A. M. Bowman, S. Xiao, and A. G. Pakhomov, "Cell permeabilization and inhibition of voltage-gated Ca(2+) and Na(+) channel currents by nanosecond pulsed electric field," (in eng), *Bioelectromagnetics,* vol. 33, no. 5, pp. 394-404, Jul 2012.
[37] V. Nesin and A. G. Pakhomov, "Inhibition of voltage-gated Na(+) current by nanosecond pulsed electric field (nsPEF) is not mediated by Na(+) influx or Ca(2+) signaling," (in eng), *Bioelectromagnetics,* vol. 33, no. 6, pp. 443-51, Sep 2012.
[38] A. G. Pakhomov *et al.*, "Excitation and electroporation by MHz bursts of nanosecond stimuli," (in eng), *Biochemical and biophysical research communications,* vol. 518, no. 4, pp. 759-764, 2019/10// 2019.
[39] G. L. Craviso, S. Choe, P. Chatterjee, I. Chatterjee, and P. T. Vernier, "Nanosecond electric pulses: a novel stimulus for triggering Ca2+ influx into chromaffin cells via voltage-gated Ca2+ channels," (in eng), *Cell Mol Neurobiol,* vol. 30, no. 8, pp. 1259-65, Nov 2010.
[40] A. G. Pakhomov, S. Grigoryev, I. Semenov, M. Casciola, C. Jiang, and S. Xiao, "The second phase of bipolar, nanosecond-range electric pulses determines the electroporation efficiency," *Bioelectrochemistry,* vol. 122, pp. 123-133, 2018/08/01/ 2018.
[41] M. Casciola *et al.*, "Cancellation of nerve excitation by the reversal of nanosecond stimulus polarity and its relevance to the gating time of sodium channels," *Cellular and Molecular Life Sciences,* vol. 76, no. 22, pp. 4539-4550, 2019/11/01 2019.
[42] A. Matiukas *et al.*, "Near-infrared voltage-sensitive fluorescent dyes optimized for optical mapping in blood-perfused myocardium," *Heart Rhythm,* vol. 4, no. 11, pp. 1441-1451, 2007/11/01/ 2007.
[43] R. J. Clarke, P. Schrimpf, and M. Schöneich, "Spectroscopic investigations of the potential-sensitive membrane probe RH421," *Biochimica et Biophysica Acta (BBA) - Biomembranes,* vol. 1112, no. 1, pp. 142-152, 1992/11/23/ 1992.
[44] M. Koch, M. Bartonek, J. Silny, B. Podesser, and D. Santer, "In-vitro study of current induced ventricular fibrillation in rabbits," *Proceedings of the 2018 Bioelectromagnetics Conference,*
[45] S. Bohl, D. J. Medway, J. Schulz-Menger, J. E. Schneider, S. Neubauer, and C. A. Lygate, "Refined approach for quantification of in vivo ischemia-reperfusion injury in the

mouse heart," *American Journal of Physiology-Heart and Circulatory Physiology,* vol. 297, no. 6, pp. H2054-H2058, 2009.
[46] C. Gabriel, *Compilation of the Dielectric Properties of Body Tissues at RF and Microwave Frequencies*. 1996, p. 272.
[47] V. G. Artemov, A. A. Volkov, N. N. Sysoev, and A. A. Volkov, "Conductivity of aqueous HCl, NaOH and NaCl solutions: Is water just a substrate?," *EPL (Europhysics Letters),* vol. 109, no. 2, p. 26002, 2015/01/01 2015.
[48] F. Varghese, J. U. Neuber, F. Xie, J. M. Philpott, A. G. Pakhomov, and C. W. Zemlin, "Low-energy defibrillation with nanosecond electric shocks," *Cardiovascular Research,* vol. 113, no. 14, pp. 1789-1797, 2017.
[49] C. D. Deakin and J. J. S. Ambler, "Post-shock myocardial stunning: A prospective randomised double-blind comparison of monophasic and biphasic waveforms," *Resuscitation,* vol. 68, no. 3, pp. 329-333, 2006/03/01/ 2006.
[50] I. Semenov, S. Xiao, D. Kang, K. H. Schoenbach, and A. G. Pakhomov, "Cell stimulation and calcium mobilization by picosecond electric pulses," *Bioelectrochemistry,* vol. 105, pp. 65-71, 2015/10/01/ 2015.
[51] B. Hille, "Ionic channels in excitable membranes. Current problems and biophysical approaches," *Biophysical Journal,* vol. 22, no. 2, pp. 283-294, 1978/05/01/ 1978.
[52] C. W. Zemlin, S. Mironov, and A. M. Pertsov, "Near-threshold field stimulation: Intramural versus surface activation," *Cardiovascular Research,* vol. 69, no. 1, pp. 98-106, 2006.
[53] R. W. Koster, P. Dorian, F. W. Chapman, P. W. Schmitt, S. G. O'Grady, and R. G. Walker, "A randomized trial comparing monophasic and biphasic waveform shocks for external cardioversion of atrial fibrillation," *American Heart Journal,* vol. 147, no. 5, pp. e1-e7, 2004/05/01/ 2004.
[54] K. A. Mowrey, Y. Cheng, P. J. Tchou, and I. R. Efimov, "Kinetics of defibrillation shock-induced response: design implications for the optimal defibrillation waveform," *EP Europace,* vol. 4, no. 1, pp. 27-39, 2002.
[55] K. A. Mowrey, I. R. Efimov, and Y. Cheng, "Membrane time constant during internal defibrillation strength shocks in intact heart: effects of Na+ and Ca2+ channel blockers," (in eng), *Journal of cardiovascular electrophysiology,* vol. 20, no. 1, pp. 85-92, 2009.
[56] V. Sharma, F. Qu, V. P. Nikolski, P. DeGroot, and I. R. Efimov, "Direct measurements of membrane time constant during defibrillation strength shocks," *Heart Rhythm,* vol. 4, no. 4, pp. 478-486, 2007.
[57] I. R. Efimov, F. Aguel, Y. Cheng, B. Wollenzier, and N. Trayanova, "Virtual electrode polarization in the far field: implications for external defibrillation," *American Journal of Physiology-Heart and Circulatory Physiology,* vol. 279, no. 3, pp. H1055-H1070, 2000.
[58] L. K. Holley and R. M. McCulloch, "Comparison of biphasic and monophasic defibrillation waveforms in an isolated rabbit heart preparation," *Cardiovascular Research,* vol. 25, no. 12, pp. 979-983, 1991.
[59] T. R. Gowrishankar, A. T. Esser, K. C. Smith, R. S. Son, and J. C. Weaver, "Intracellular electroporation site distributions: Modeling examples for nsPEF and IRE pulse waveforms," in *2011 Annual International Conference of the IEEE Engineering in Medicine and Biology Society*, 2011, pp. 732-735.

[60] K. C. Melikov, V. A. Frolov, A. Shcherbakov, A. V. Samsonov, Y. A. Chizmadzhev, and L. V. Chernomordik, "Voltage-induced nonconductive pre-pores and metastable single pores in unmodified planar lipid bilayer," (in eng), *Biophysical journal,* vol. 80, no. 4, pp. 1829-1836, 2001.
[61] P. T. Vernier, Y. Sun, L. Marcu, S. Salemi, C. M. Craft, and M. A. Gundersen, "Calcium bursts induced by nanosecond electric pulses," *Biochemical and Biophysical Research Communications,* vol. 310, no. 2, pp. 286-295, 2003/10/17/ 2003.
[62] R. S. Son, K. C. Smith, T. R. Gowrishankar, P. T. Vernier, and J. C. Weaver, "Basic Features of a Cell Electroporation Model: Illustrative Behavior for Two Very Different Pulses," *The Journal of Membrane Biology,* vol. 247, no. 12, pp. 1209-1228, 2014/12/01 2014.
[63] Y. T. Wang, I. R. Efimov, and Y. Cheng, "Electroporation induced by internal defibrillation shock with and without recovery in intact rabbit hearts," *American Journal of Physiology - Heart and Circulatory Physiology,* vol. 303, no. 4, pp. H439-H449, 2012.
[64] J. U. Neuber, F. Varghese, A. G. Pakhomov, and C. W. Zemlin, "Using Nanosecond Shocks for Cardiac Defibrillation," *Bioelectricity,* vol. 1, no. 4, pp. 240-246, 2019/12/01 2019.
[65] J. E. Azarov, I. Semenov, M. Casciola, and A. G. Pakhomov, "Excitation of murine cardiac myocytes by nanosecond pulsed electric field," *Journal of Cardiovascular Electrophysiology,* vol. 30, no. 3, pp. 392-401, 2019.
[66] A. G. Pakhomov and O. N. Pakhomova, "The interplay of excitation and electroporation in nanosecond pulse stimulation," *Bioelectrochemistry,* vol. 136, p. 107598, 2020/12/01/ 2020.
[67] A. G. Pakhomov, E. Gianulis, P. T. Vernier, I. Semenov, S. Xiao, and O. N. Pakhomova, "Multiple nanosecond electric pulses increase the number but not the size of long-lived nanopores in the cell membrane," (in eng), *Biochimica et biophysica acta,* vol. 1848, no. 4, pp. 958-966, 2015.
[68] E. C. Gianulis, M. Casciola, C. Zhou, E. Yang, S. Xiao, and A. G. Pakhomov, "Selective distant electrostimulation by synchronized bipolar nanosecond pulses," *Scientific Reports,* vol. 9, no. 1, p. 13116, 2019/09/11 2019.
[69] E. B. Rosa, *The self and mutual inductances of linear conductors* (no. 80). US Department of Commerce and Labor, Bureau of Standards, 1908.
[70] S. W. Ellingson, "Electromagnetics," vol. Vol. 1Blacksburg, VA: VT Publishing, 2018.
[71] C. ZEMLIN, S. MIRONOV, and A. PERTSOV, "Delayed Success in Termination of Three-Dimensional Reentry," *Journal of Cardiovascular Electrophysiology,* vol. 14, no. s10, pp. S257-S263, 2003.
[72] N. Chattipakorn, P. C. Fotuhi, and R. E. Ideker, "Prediction of defibrillation outcome by epicardial activation patterns following shocks near the defibrillation threshold," (in eng), *J Cardiovasc Electrophysiol,* vol. 11, no. 9, pp. 1014-21, Sep 2000.
[73] A. G. Pakhomov *et al.*, "Cancellation of cellular responses to nanoelectroporation by reversing the stimulus polarity," *Cellular and Molecular Life Sciences,* journal article vol. 71, no. 22, pp. 4431-4441, November 01 2014.
[74] E. C. Gianulis, M. Casciola, S. Xiao, O. N. Pakhomova, and A. G. Pakhomov, "Electropermeabilization by uni- or bipolar nanosecond electric pulses: The impact of extracellular conductivity," *Bioelectrochemistry,* vol. 119, pp. 10-19, 2018/02/01/ 2018.